

Looking for a vectorlike B quark at the LHC using jet substructure

Debajyoti Choudhury,^{*} Kuldeep Deka[†], and Nilanjana Kumar[‡]

Department of Physics and Astrophysics, University of Delhi, Delhi 110007, India



(Received 6 April 2021; accepted 16 July 2021; published 5 August 2021)

Vectorlike quarks have been shown to resolve certain longstanding discrepancies pertaining to the bottom sector. We investigate, here, the prospects of identifying the existence of a topless vectorlike doublet (B, Y) , as is preferred by the electroweak precision measurements. Concentrating on single production, *viz.* $B\bar{B}$ with $B \rightarrow b + Z/H$ subsequently, we find that the fully hadronic decay-channel is susceptible to discovery provided jet substructure observables are used. At the 13 TeV LHC with an integrated luminosity of 300 fb^{-1} , a modest value of the chromomagnetic transition moments allows for the exclusion of $M \lesssim 1.8(2.2) \text{ TeV}$ in the Z and H channels respectively.

DOI: 10.1103/PhysRevD.104.035004

I. INTRODUCTION

Over the last three decades, the Standard Model (SM) has been vindicated to an unprecedented degree of accuracy by several experiments, taken singly or in conjunction. These include, but are not limited to, the electroweak precision tests [1], the measurement of the top mass [2] culminating with the discovery of the Higgs particle [3,4]. Yet, certain anomalies persist, starting from the 2.9σ discrepancy in the forward-backward asymmetry (A_{FB}^b) of the b -quark at LEP/SLC [1], a newly updated 4.2σ deviation in the anomalous magnetic moment of the muon [5] to the more recent ones in both charged and neutral-current decays of B -mesons [6]. These are accompanied by the SM's failure in explaining neutrino masses and mixings on the one hand and, on the other, to address questions related to the lightness of the Higgs or the preponderance of matter over antimatter.

Many diverse scenarios going beyond the SM have been proposed to address such issues. Near-ubiquitous in all of them are extra fermion fields. With most such fields not being gauge-singlets, non-observation at collider experiments can only mean that they are very heavy. A chiral assignment of quantum numbers (as is the case within the SM) for heavy fields would imply uncomfortably large Yukawa couplings and, hence, an acute tension with not only the electroweak precision tests, but also with Higgs

production and decay. Nonchiral fermions, since they allow for gauge-invariant bare mass terms, easily evade such restrictions.

Such vectorlike assignments abound in many diverse scenarios [7,8]. Even the simplest supersymmetric construct has them in the form of the Higgsinos. Additional vectorlike matter may arise in the quest of enlarging the symmetry, whether gauge [9–14], or space-time [15], with the Dirac-like gauginos in the latter suppressing pair production channels and cascade decays that are possible for the usual Majorana-gaugino theories. Similarly, extending the Higgs-sector to obtain an R -symmetric theory has very interesting ramifications [16]. Vectorlike matter can also help raise the mass of the SM-like Higgs [17,18] in supersymmetric theories or to alleviate the little hierarchy problem [19]. And, finally, many of the problems that beset gauge-mediated breaking of supersymmetry may be alleviated too [20–23].

Nonchiral fermions abound in nonsupersymmetric scenarios as well, historically interesting examples being provided by models wherein electroweak symmetry breaking proceeds dynamically through the condensation of top quarks (or its partners) [24–26]. And while they are, almost by definition, ubiquitous in any extra-dimensional model wherein the SM fields venture into the bulk (in the form of Kaluza-Klein excitations), they are also present in composite Higgs [27–33], as well as little Higgs scenarios [34–40], or those advocating a Higgs-portal to obtain the correct relic abundance for dark matter [41–43].

As argued above, to address different issues, a plethora of vectorlike fermions have been advocated, either singly¹ or in combinations. For example, these have been invoked to explain the longstanding discrepancy in the muon

^{*}debchou.physics@gmail.com

[†]kuldeepdeka.physics@gmail.com

[‡]nilanjana.kumar@gmail.com

Published by the American Physical Society under the terms of the Creative Commons Attribution 4.0 International license. Further distribution of this work must maintain attribution to the author(s) and the published article's title, journal citation, and DOI. Funded by SCOAP³.

¹Note that anomaly cancellation is not an issue.

anomalous moment [44,45] or to address flavor discrepancy pertaining to b -quarks [46–49]. In the present analysis, we would be concentrating on a single such vectorlike quark (VLQ) doublet. Since substantial mixings with the SM quarks are liable to set up too large a FCNC, we assume that it is only with the third-generation that it may participate in Yukawa interactions.² Such scenarios had been shown, in Ref. [50], to explain the longstanding problem with A_{FB}^b without coming into conflict with any other constraint pertaining to electroweak precision tests. Interestingly, while, of the two quantum number assignments proposed in Ref. [50], one preferred relatively light VLQs (and, hence, would be disfavoured by the absence of signals at the LHC), the other is not only more attractive on theoretical grounds, but also preferred VLQs in the TeV-range.

In the present paper, we are concerned with a VLQ that, among other things, is useful in ameliorating the longstanding tension between the global fits to electroweak precision tests [1] and A_{FB}^b . The latter, taken in conjunction with the $Z \rightarrow \bar{b}b$ branching ratio and the forward-backward asymmetry for the charm-quark requires a substantial new physics effect in the b -sector [51]. This is best brought forward by considering an effective $Z\bar{b}b$ vertex parametrized by

$$g_{L,R} \rightarrow g_{L,R} + \delta g_{L,R}$$

where the tree-level SM couplings are $g_L = 1/2 + s_W^2/3 \approx -0.42$ and $g_R = s_W^2/3 \approx -0.077$, with s_W being the Weinberg angle. The deviations $\delta g_{L,R}$ could arise either from quantum corrections (as in the SM) or new physics effects. In terms of the effective couplings, the expressions for $R_b \equiv \Gamma(Z \rightarrow \bar{b}b)/\Gamma(Z \rightarrow \text{hadrons})$ and A_{FB}^b are approximated to the leading order by

$$\begin{aligned} R_b &= R_b^{\text{SM}}(1 - 1.820\delta g_L + 0.336\delta g_R), \\ A_{FB}^b &= A_{FB}^{b,\text{SM}}(1 - 0.164\delta g_L - 0.8877\delta g_R). \end{aligned} \quad (1)$$

With the measured value of A_{FB}^b being substantially less than the SM prediction, but that for R_b being marginally higher, a positive δg_R is called for. As was argued in Ref. [50], the required magnitude of deviation is too large to be attributable to loop corrections. On the other hand, a tree-level δg_R (along with a tiny, but welcome, δg_L) is naturally generated if the b quark mixes with a VLQ that is part of a $SU(2)_L$ -doublet. The standard choice of the hypercharge ($Y = 1/6$) would require a very large δg_R , such that the sign of the effective g_R is reversed [50]. The ensuing large mixing has severe ramifications in

²In the absence of any such mixing, the lighter of the two VLQs would be stable, and, hence run afoul of constraints from the nonexistence of exotic bound states.

low-energy physics. This, along with LHC constraints as well as several theoretical considerations [50] implies that $Y = -5/6$ (leading to a topless doublet, $\psi_{L,R}^T = (BY)$) is favoured.

The production and subsequent decays of such VLQs at the LHC has been widely studied in the literature and constraints are imposed from nonobservation [52–59]. While QCD-driven pair-production is bereft of any model-dependence and, naively, expected to be the dominant mode at the LHC, for large masses, the kinematical suppression as well as the suppression due to falling gluon densities quickly limit the sensitivity. Single production, being model-dependent, has the added advantage of providing a window to the ultraviolet completion. A particularly interesting set of couplings that this may probe are the transition magnetic moments, whether of electroweak nature or chromomagnetic. Simple strategies to probe this was developed in Refs. [60,61] and, subsequently, exploited by the CMS collaboration [59,62] to look at a singly-produced VLQ decaying into its SM counterpart and a photon. Somewhat analogous is the case of a VLQ decaying into a bottom quark and a Z [54] or a Higgs boson [56].

While both the pair-production and single-production modes have already been used by the ATLAS and CMS collaboration [56,57,63–65] to impose a lower limit of $m_B \gtrsim 1\text{--}1.3$ TeV [66] for such a VLQ coupling primarily to the b -quark, it still behoves us to look for complementary channels. To this end, we consider the production of such a VLQ, in association with b quark and subsequent decays of VLQ into either a $b + Z$ or a $b + H$ pair, as these modes are associated with a very substantial branching fraction for a large part of the parameter space. With a large m_B implying that both the daughters would be highly boosted, the Z (or H) is more likely to manifest itself as a single fatjet rather than two resolved jets. Notwithstanding the subtleties involved in the use of jet substructures, the much larger hadronic branching ratio for the Z and H renders these channels very competitive with the leptonic ones. While fatjet signatures have been investigated in the context of VLQs [67–70], ours is the first effort to use it for this all hadronic final state.

The rest of the paper has been structured as follows. We begin, in Sec. II, by setting up the formalism and detailing the relevant aspects of the parameter space that we would explore. This is followed, in Sec. III, by a brief recounting of jet substructure as this would be the bedrock of our analysis. The details of the analysis are presented in Sec. IV followed by the concluding Sec. V.

II. THEORETICAL BACKBONE

As we have explained in the preceding section, we would be concentrating on a nonchiral colored $SU(2)_L$ fermion field with a hypercharge of $-5/6$, viz., $\Psi_{L,R} \equiv (B', Y')_{L,R}^T$.

With there being no charge-2/3 quark, several constraints are automatically relaxed. Our motivation being to develop a particular search algorithm, we desist from incorporating the other fields included in Ref. [50], and begin by setting up the formalism and reviewing some immediate consequences.

A. The model

The kinetic (including gauge interactions) term for the $\Psi_{L,R}$ fields are exactly analogous to those for the SM quarks. Being vectorial in nature, these quarks can acquire a bare mass M . Furthermore, in view of the strong constraints from flavor physics, the only Yukawa coupling allowed to Ψ_L is that with the SM field b_R alone (with gauge invariance preventing any such term of Ψ_R). Denoting all the gauge (mass) eigenstates by primed (unprimed) fields, the relevant additional term in the Lagrangian can be written as

$$-\mathcal{L} \ni y_1 \bar{Q}_{3L} b'_R H + y_2 \bar{\Psi}'_L b'_R H + M \bar{\Psi}'_L \Psi'_R + \text{H.c.}, \quad (2)$$

where H is the SM Higgs doublet. After spontaneous symmetry breaking, the relevant mass terms are expressible as

$$\mathcal{L}_{\text{mass}} \ni [\bar{b}'_L \bar{B}'_L] \mathcal{M} \begin{bmatrix} b'_R \\ B'_R \end{bmatrix}, \quad \mathcal{M} = \begin{bmatrix} y_1 v & 0 \\ y_2 v & M \end{bmatrix} \quad (3)$$

where v is the SM vev. For the sake of simplicity, we have neglected here the much smaller terms connecting b' to s' , d' . Considerations of electroweak precision tests (more specifically, the ρ -parameter) stipulate that $y_2 v \ll M$. The mass matrix can be diagonalized by a biunitary transformation defined by

$$\begin{bmatrix} b_{L,R} \\ B_{L,R} \end{bmatrix} = \begin{bmatrix} c_{L,R} & -s_{L,R} \\ s_{L,R} & c_{L,R} \end{bmatrix} \begin{bmatrix} b'_{L,R} \\ B'_{L,R} \end{bmatrix} \quad (4)$$

where $c_{L,R} \equiv \cos \theta_{L,R}$ and $s_{L,R} \equiv \sin \theta_{L,R}$. The physical masses and the mixing angles are given by

$$m_b \approx y_1 v \left[1 + \frac{y_2^2 v^2}{M^2} \right]^{-1/2}, \quad \tan \theta_R \approx \frac{-y_2 v}{M},$$

$$\tan \theta_L \approx \frac{-y_1 y_2 v^2}{(M^2 + y_2^2 v^2)}. \quad (5)$$

It is worth remembering that, for small mixing angles,

$$s_L \approx \frac{m_b}{M} s_R. \quad (6)$$

It is easy to ascertain (for example, from the very structure of \mathcal{M}^2) that

$$m_Y^2 = M^2 = m_B^2 c_R^2 + m_b^2 s_R^2. \quad (7)$$

While $m_B > m_Y$, the smallness of the ratio $(y_2 v/M)$ ensures that the splitting is too small to permit $B \rightarrow Y + W^-$, and even $B \rightarrow Y + \bar{f} + f'$ is very small indeed. The electroweak interactions of the mass-eigenstate B are obtained trivially. Restricting ourselves to those that could, potentially, lead to the decay of the B , we have

$$\mathcal{L}_{\mathcal{W}}^{(B)} = \frac{-g_{S_L}}{\sqrt{2}} \bar{t} \gamma^\mu P_L B W_\mu^+ + \text{H.c.}$$

$$\mathcal{L}_{\mathcal{Z}}^{(B)} = \frac{g}{2c_W} \bar{b} \gamma^\mu [2s_L c_L P_L + s_R c_R P_R] B Z_\mu + \text{H.c.}$$

$$\mathcal{L}_{\mathcal{H}}^{(B)} = \frac{-g_{S_R c_R}}{2m_W} \bar{b} [M_B P_L + m_b P_R] B H + \text{H.c.}, \quad (8)$$

where $P_{L,R} = (1 \mp \gamma_5)/2$ and g is the $SU(2)_L$ gauge coupling. The mixing of quark fields of different isospin (and hypercharge) that generated the interactions of Eq. (8) would also result in an alteration of the effective gauge couplings of the eigenstates dominated by the SM quarks. In particular, both of the $\bar{b}bZ$ couplings $g_{L,R}(b)$ receive non-zero corrections, leading, in turn, to corrections in R_b and A_{FB}^b [see Eq. (1)]. The most important parameter, in this context, turns out to be s_R [50], with s_L playing only a subservient role is ensuring a correct R_b . While observables such as R_c and $\Gamma_{\text{had}}(Z)$ are affected too, these play even more subservient roles. Thus, R_b and A_{FB}^b can be used to delineate the appropriate part of the parameter space. With the present scenario relating s_L and s_R [with $s_L \ll s_R$, *vide* Eq. (6)], only one of them is a free parameter. Furthermore, with the aforementioned observables being essentially independent of m_B (since one-loop corrections due to the new quarks are too small to be of any consequence), the observables under discussion constrain only s_R .

We see from Eq. (5) that a perturbative limit on the Yukawa coupling y_2 would translate to a bound on s_R , scaling approximately as m_B^{-1} . However, stronger constraints arise from observables such as A_{FB}^b and R_b , as discussed in the preceding section. Although the other precision measurements, such as $A_b \equiv [(g_L^b)^2 - (g_R^b)^2] / [(g_L^b)^2 + (g_R^b)^2]$ and R_c too contribute to the constraints, these have relatively minor roles³ to play as far as this sector is concerned. For completeness, we quote here the ‘‘SM’’ values of the parameters, defined as the values inferred from the global best-fit [2] to all electroweak precision observables (with quantum corrections incorporated). Restricting ourselves, for brevity’s sake, to the most relevant ones, these are $R_b^{\text{SM}} = 0.21576(0.21629 \pm 0.00066)$, $A_{FB}^{\text{SM}} = 0.1034(0.0992 \pm 0.0016)$, $A_b^{\text{SM}} = 0.9348(0.923 \pm 0.020)$,

³It should be remembered that with the beams being unpolarized at LEP, A_b and A_{FB}^b differ essentially by a factor of A_e . At the SLD, though, they differed on account of the polarization, but in a straightforward manner.

$R_c^{\text{SM}} = 0.17227(0.1721 \pm 0.003)$, where the numbers in the parentheses refer to the direct experimental measurements [71]. While all the electroweak precision measurements were considered in Ref. [50] in deriving the preferred values of the parameters, Ref. [7] concentrated on R_b and A_{FB}^{SM} in obtaining the “best-fit” value of s_R , along with error bands. It should be realized, though, that the other precision electroweak measurements [71], too have an important role to play. In particular, the oblique parameter T (equivalently ρ), receives an additional contribution proportional to $s_R^2 m_B^2$ and this translates to a stringent bound on $s_R \propto m_B^{-1}$ especially for larger m_B values. The exact results are shown in [7] where experimental value of ΔT and ΔS are taken to be 0.07 ± 0.08 and 0.04 ± 0.07 from [2].

Typically, for $m_B \lesssim 1$ TeV, it is the $Z \rightarrow b\bar{b}$ observables that impose stronger constraints, while for $m_B \gtrsim 1$ TeV, it is the constraints from the oblique parameters which are stronger, and, for $m_B \gtrsim 1.7$ TeV, these tend to rule out the values that best fit the $Z \rightarrow b\bar{b}$ observables [7]. Being interested primarily in $m_B \gtrsim 1.2$ TeV, we use the corresponding 1σ upper limits.

The presence of such exotic quarks would also serve to alter the effective gluon-gluon-Higgs and photon-photon-Higgs vertices, nominally enhancing the former and suppressing the latter (on account of destructive interference with the W -loop). However, with B being vectorlike, its contribution to either loop can only be proportional to the mass term connect it to the SM quark. In other words, in the limit of large m_B , the new physics contribution is proportional to s_R ; even for its maximum possible value of 0.18 (as constrained by the Z -pole observables), a maximal enhancement of 3.2% is admissible in the ggH vertex and a maximal suppression of 0.2% in the $\gamma\gamma H$ vertex. The partial decay width for $H \rightarrow b\bar{b}$ suffers a change on two accounts, primarily from the alteration of the $Hb\bar{b}$ vertex (by a factor of c_R^2) due to the mixing and, to a much smaller extent, the aforementioned change in $H \rightarrow gg$. The cumulative effect is a suppression by less than 6.4%. Consequently, the Higgs branching ratios into other final states are enhanced, at most, by an extra 3.8%. On the experimental side, the production through gg fusion has an uncertainty of about 9% and $H \rightarrow b\bar{b}$ has an uncertainty of 10% [72]. If we consider the production of H through vector-boson fusion, then the uncertainty in the production cross section is close to 20% [72]. In summary, the LHC measurements in the Higgs sector leads to virtually no worthwhile constraint on this sector. The situation would, of course improve considerably at the HL-LHC.

A very important issue is that of FCNCs involving either of the down- or strange-quarks. The existence of such terms would lead to enhancement of suppressed decays (that, normally, occur only at the loop-level) as also diverse meson-antimeson oscillations. As we have already mentioned in Sec. I, such FCNCs can be suppressed if one posits that the B mixes only with the b . Of course, the fact

that, in general, mass terms such as $m_{bs}\bar{b}s$ or $m_{db}^*\bar{d}b$ are nonzero (in the flavor basis) one would still expect some FCNCs involving the light flavors. The strength thereof would, however, be suppressed. Given the structure of the Cabibbo-Kobayashi-Maskawa matrix, these suppressions, barring large cancellations in the flavor sector, would be $\mathcal{O}(\lambda^4)$ or even more severe, where λ is the Cabibbo angle. Such a minimal texture in the quark mixing matrix (as indicated above) is, thus, more than enough to protect one from the FCNC bounds. Indeed, the texture could be perturbed a little to induce tiny tree-level FCNCs connecting the b to the d/s in an effort to address the recently observed anomalies in B -decays. However, since the latter also seemingly involve lepton-flavour violations, we deliberately desist from treading that path.

B. Transition chromomagnetic moment

A consequence of the mixing between fields with different quantum numbers has been the generation of Z -mediated flavor-changing neutral currents. This also explains why the mixing in the left-handed sector is allowed to be much larger than in the right-handed one. Understandably, the extant $SU(3)_c \otimes U(1)_{em}$ gauge symmetry precludes any such tree-level currents coupling to the photon or the gluons. This, however, does not prevent the generation, as a result of quantum corrections, of gauge invariant terms of the form

$$\mathcal{L}_g = \frac{g_s}{2\Lambda} G_{\mu\nu}^a \bar{b} \sigma^{\mu\nu} T^a [\kappa_L^b B_L + \kappa_R^b B_R] + \text{H.c.}, \quad (9)$$

where g_s is the strong coupling constant and $G_{\mu\nu}^a$ is the field strength tensor for the gluon. Analogous to electromagnetic transition moments, the dimensionless constants $\kappa_{L,R}$ are determined by the couplings and mass spectrum of the full theory, including all those above the mass scale Λ that have been integrated out. For the sake of simplicity, we consider these to be real and equal, thereby also eliminating additional sources of CP violation. For our purposes, only the magnitude of $\kappa \equiv \kappa_{L,R}$ is relevant (for more details see Ref. [73] and references therein), and in the absence of any theoretical knowledge, we shall only assume a phenomenologically guided limit of $|\kappa| < 0.8$.

C. Decay width and branching ratio

With its isospin partner being nearly degenerate with it and all the SM particles being much lighter, B decays are dominated by two-body final states, namely $B \rightarrow bg$, $B \rightarrow Zb$ and $B \rightarrow Hb$. The first of these proceeds through the chromomagnetic moment κ . The other two are driven by the mixings⁴ $s_{L,R}$, and for a very large m_B , have nearly equal partial widths, a consequence of the Goldstone

⁴Since $s_L \ll s_R$, the decay $B \rightarrow Wt$ is highly suppressed.

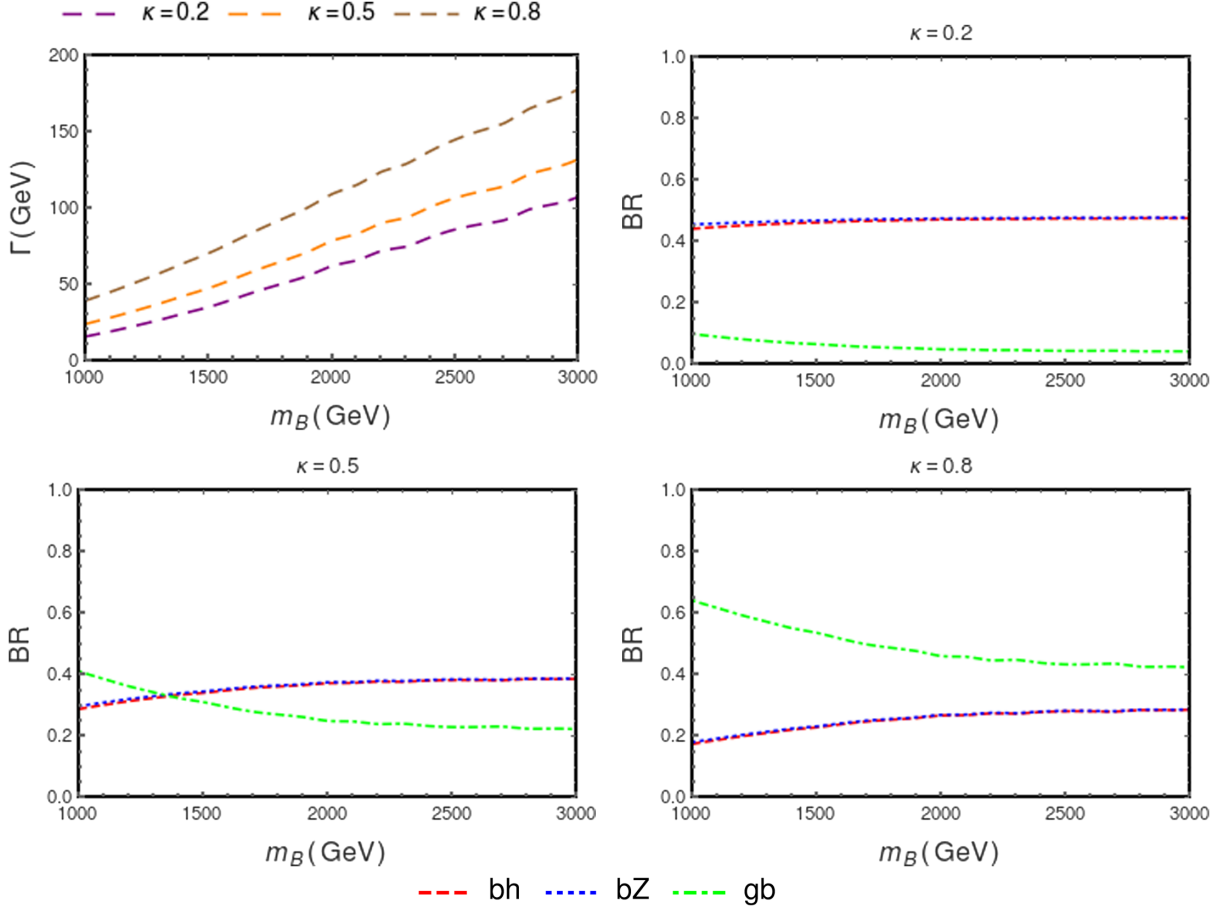


FIG. 1. The upper left plot shows total decay width as a function of m_B using the limit on s_R mainly coming from oblique parameters. The other three plots show the branching ratio of B to bH , bZ and bg as a function of m_B , for three different values of κ .

equivalence theorem. For relatively modest values of m_B , though, the two may differ by as much as 20%.

In Fig. 1, we depict the total decay width and the major branching fractions for a value of s_R that best fits A_{FB}^b while being consistent with the oblique parameter constraints. As the top left panel shows, even for a very large value of $\kappa \equiv \kappa_{L,R}$, the ratio $\Gamma/m_B \lesssim 0.06$, thereby validating the narrow width approximation. We would be using smaller κ values, though. In this paper we study the case of a particularly heavy B decaying to Z/H and a b -jet, with the Z/H manifesting itself as a fatjet. Before going to the detailed analysis, we briefly discuss, in the next section the jet substructure techniques that are useful to detect the properties of such a fatjet.

III. JET-SUBSTRUCTURE TECHNIQUES

Jets are nothing but a cluster of hadrons produced as a result of showering and hadronization following high energy particle collisions and identified using an appropriate jet reconstruction algorithm. With the B quark being very heavy, and its daughters (say, b and Z/H) relatively light, the latter would, typically, be highly boosted.

Consequently, the angular separation between the subsequent decay products (of the Z/H in this case) would tend to be small. While this would still not present a problem for the detection of $Z \rightarrow \mu^+\mu^-, e^+e^-$, for the dominant decay modes, *viz.*, $Z \rightarrow q\bar{q}$, the closeness would, typically, result in the ensuing jets merging into a single, albeit fat, jet. Fat jets (along with their subjet structures) have been studied in the context of many search strategies, such as those for strongly interacting W bosons [74,75], supersymmetric particles [76,77], heavy resonances decaying to strongly boosted top quarks [78], as well as the Higgs production in association with a W/Z [79,80].

To reconstruct the $W/Z/H$ jets, different algorithms have been used in the literature, whether it be anti- k_T [81], Cambridge-Aachen [82] or a combination of both [75]. In the present study, the hadrons are clustered using the⁵ anti- k_T algorithm [83]. We investigate the variation of the signal efficiency and the reconstruction of jet substructure variables with two choices of the distance parameter R in the

⁵The specificity of the hierarchical clustering renders this algorithm more useful for the kind of fatjets that we are interested in.

next section. This distance parameter, also known as the jet radius, is an angular cutoff such that a splitting of a parent particle to two daughter particles $P \rightarrow ij$ will never be combined by the jet algorithm if $\Delta R_{ij} > R$ where, $\Delta R \equiv \sqrt{(\Delta\eta)^2 + (\Delta\phi)^2}$ is the (angular) separation in the azimuth-rapidity plane. Not only should the fatjet arising from the hadronic decay of the $Z(H)$ have a reconstructed jet mass close to $m_Z(m_H)$, but it is also expected to resolve into a two-prong substructure. However, some of these properties can be degraded on account of extraneous objects (owing to QCD radiation) that can vitiate jet-reconstruction. Consequently, one needs to use appropriate jet grooming techniques that help in eliminating soft and large-angle QCD radiation. Of many such, we choose to use the *jet pruning* algorithm [84,85], a popular choice for reconstructing $W/Z/H$ fatjets [81]. While alternative algorithms such as *softdrop* [86] have also been used [87], it has been shown that the discrimination afforded is very similar [88].

A. Jet pruning

In a typical event at the LHC, a very large number of hadronic entities impinge on the detectors. Furthermore, there exist color reconnections between objects emanating from disparate fundamental processes, hard or soft. The jet reconstruction algorithm, being statistical in nature, cannot always effect an exact differentiation. Pruning is one of the jet-grooming methods to remove those constituents from the jets that carry no significant or useful information. For example, the (invariant) mass of a jet ought to reflect the mass of the primary object, small for a pure QCD jet, and close to the particle mass for a heavy particle. This is facilitated by removing the soft yet large angle constituents of the jet because of the statistically smaller likelihood of their being correlated with the energetic constituents of the jet. Mathematically, at each merging step ($j + k \rightarrow l$), we define two constraints given by

- (i) softness: $p_k/p_l < z_{\text{cut}}$ for ($p_k < p_j$), and
- (ii) separation: $\Delta R_{jk} > R_{\text{cut}}$.

If both these conditions are met, then we prune (remove) the constituent k and proceed for the next merging. A larger (smaller) value for $z_{\text{cut}}(R_{\text{cut}})$ will result in more aggressive pruning. Clearly, the level of pruning is largely determined by the less aggressive of the two parameters. As for z_{cut} and R_{cut} , the parameters of the pruning algorithm, we choose the default values,⁶ namely, $z_{\text{cut}} = 0.1$ and $R_{\text{cut}} = 0.5$ as suggested in Ref. [84]. The pruned jet mass, m_j , is computed from the sum of the four-momenta of the components that remain after pruning, and the resultant jet is considered to be a $Z(H)$ -fatjet candidate if m_j is

⁶While using a R_{cut} that is dependent on the natural angular size of the jet, viz, m_j/p_j is tempting, this introduces a degree of sophistication not commensurate with the nature of our analysis.

commensurate with the $Z(H)$ -mass within the detector resolution limits. And while the irreducible SM backgrounds (with a high-momentum $Z(H)$) would also show similar characteristics, the overwhelmingly stronger pure QCD background would, typically, have jets with much lower masses.

B. N-subjettiness

Heavy VLQ decays tend to produce top quarks and/or a W, Z , or a Higgs boson with high momenta, causing their respective decay products to merge into a single fat jet [89–91]. If the latter is to be resolved into subjets, a naturally important question relates to the precise number of such putative subjets. A good measure of this is N -subjettiness [92] defined as

$$\tau_N = \frac{1}{d_0} \sum_k p_{T,k} \min(\Delta R_{1k}, \Delta R_{2k}, \dots, \Delta R_{Nk}) \quad (10)$$

where N is the number of candidate subjets of the jet to be reconstructed. k runs over constituent particles in a given jet with $p_{T,k}$ being their transverse momenta and $\Delta R_{j,k}$ the angular separation between a candidate subjet j and a constituent particle k . Furthermore,

$$d_0 = \sum_k p_{T,k} R_0 \quad (11)$$

where R_0 is the characteristic jet-radius. Physically, τ_N provides a dimensionless measure of whether a jet can be regarded to be composed of N -subjets. In particular, ratios τ_N/τ_{N-1} are powerful discriminants between jets predicted to have N internal energy clusters and those with fewer clusters. As applied to our case, jets coming from the hadronic decays of the $Z(H)$ tend to have lower values for the ratio $\tau_{21} \equiv \tau_2/\tau_1$ as compared to QCD or top-jets and, hence, constitutes a good discriminator.

IV. COLLIDER SIGNATURES

As discussed above, we are interested in the single production of the vectorlike quark B at the LHC. Several parton-level processes may contribute. In decreasing order of the production cross sections, these are

- (i) $bg \rightarrow B$,
- (ii) $bg \rightarrow Bg$
- (iii) $q\bar{q} \rightarrow \bar{b}B$ and $gg \rightarrow \bar{b}B$,
- (iv) $bg \rightarrow (Z/H)B$,

with the conjugate process being understood in each case. We would be concentrating here on the third, viz., $\bar{b}B$ production (dominated by the gluon-fusion contribution). The reason is easy to understand. Since we would be concentrating on fully hadronic cascade decays of the B , each of these channels suffer from large QCD backgrounds. The $\bar{b}B$ mode, with $B \rightarrow b + Z/H$ would admit two hard

b -tagged jets, thereby offering additional discriminatory power.

To this end, we begin by a detailed discussion, in the next subsection, of the process $pp \rightarrow bB, B \rightarrow Zb$ involving the Z -fatjet. The other channel, namely $pp \rightarrow bB, B \rightarrow Hb$ shows analogous behavior and, hence, for the sake of brevity, we do not provide details but only highlight the differences.

A. Signal: $pp \rightarrow bB, B \rightarrow Zb(Hb)$

We calculate the leading-order on-shell production cross-section⁷ in the five flavor scheme (5FS), using the NNPDF23LO1 [93] parton distributions holding the factorization scale to $\mu_F^2 = 2m_B^2$. The final state, being comprised of jets only, largely depends on additional jet radiations. Within this scheme, inclusion of the next-to-leading order effects suppresses the cross sections by a factor ~ 0.9 [94] over the mass-range of interest to us. It should also be pointed out at this stage that owing to the relatively modest reach of this mode, uncertainties due to the choice of the parton distributions are relatively small.

In Fig. 2, we plot, as a function of m_B , the product $\sigma(pp \rightarrow bB) \times \text{BR}(B \rightarrow bZ)$. The production cross section is largely dominated by gluon fusion, with both the leading and the subleading (i.e., $q\bar{q} \rightarrow bB$) contributions scaling as κ^2 . On the other hand, increasing κ would also enhance the partial width $\Gamma(B \rightarrow bg)$, thereby suppressing the branching fraction for the decay mode of interest, viz., $B \rightarrow bZ$. This explains the relatively slow growth of the product with κ in Fig. 2. As a reference point, we choose to work with a benchmark value of $\kappa = 0.5$. Analogously, our benchmark points (BP) in the mass-axis read $m_B = 1.2, 1.8$ and 2.2 TeV. At the very end, though, we will present the reach in the m_B - κ plane.

The signal, thus, comprises of a pair of b -jets accompanied by a Z , whose high momentum would, typically, imply that its decay products coalesce into a further fatjet. Of the two putative b -tagged jets, one would, typically, be attributed with a transverse momentum similar in magnitude and in a direction nearly opposite to that of the fat- Z . If an excess in this channel is seen, m_B could, presumably, be reconstructed from such pairings.

The second mode, viz., $pp \rightarrow Bb \rightarrow Hbb$, apart from having a nearly identical strength, also has a very similar event topology. The only difference is that, owing to a slightly higher mass of the H (as compared to the Z), its momentum would be marginally smaller and the fraction of events being identified as a fatjet a little lower.

⁷As discussed earlier, the ratio of the decay width and the mass of B in this model is, at best, 6%. Consequently, even for the full calculation of $pp \rightarrow b\bar{b}Z$, the contribution from the interference of the SM amplitude with the B -mediated one (including possible contributions from an off-shell B) is very small, and is further suppressed once all kinematic cuts are imposed.

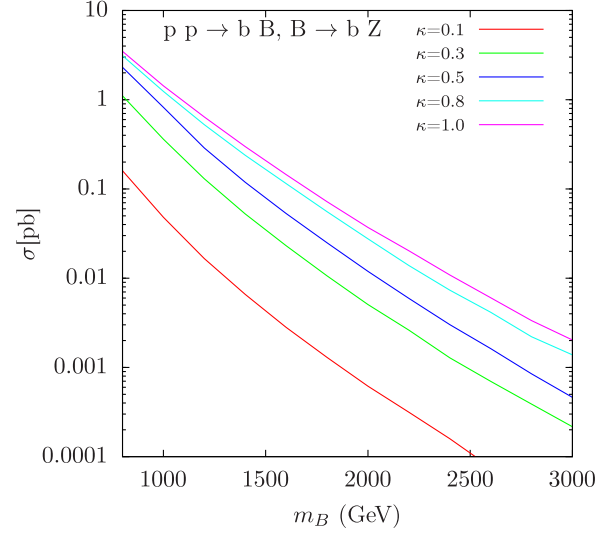


FIG. 2. The LO cross section in 5FS (using NNPDF23LO1) for $pp \rightarrow Bb \rightarrow Zbb$ at 13 TeV LHC for different values of κ . The cross sections for $pp \rightarrow Bb \rightarrow Hbb$ are virtually the same, owing to a nearly identical branching ratio, as in Fig. 1. We choose the value of s_R from Fig. 1(left) as a function of vectorlike B mass.

B. Backgrounds

While the SM backgrounds to the two aforementioned signal channels are similar, they, understandably, contribute differently in the two cases. We begin by discussing the case that suffers larger backgrounds, namely the $Zb\bar{b}$ channel. The major SM backgrounds arise from the processes detailed below.

- (i) W/Z production accompanied by multijets: As with the signal, the fatjet would arise, mostly, from the hadronic decays of the vector boson, with a rather subdominant contribution from events wherein some of the jets accompanying the W/Z are reconstructed as a fatjet. While the corresponding SM cross sections are very large, viz., for Z + jets, it is 6.3×10^4 pb (NNLO) [95,96] and 1.95×10^5 pb (NLO) for W + jets [97], note that requiring these additional jets to be b -tagged would result in a severe suppression.
- (ii) $t\bar{t}$ + jets: If the radius parameter R is small enough, then the two-prong hadronic decay of one of W 's emanating from the top decay could be reconstructed as a fatjet. Despite the smaller production cross section (≈ 990 pb at N³LO [98]), this would be expected to be a major background owing to the automatic presence of two b -jets.
- (iii) QCD n -jets ($n \geq 4$) with none being b - or c -like: This, of course, is very large indeed ($\sim 10^8$ pb). And even with the requirement that two (or more) of these jets should reconstruct to close to m_Z , the wide jetmass distribution means that a non-negligible fraction would satisfy the cuts. However, with the cross section being an even stronger function of p_T^{\min}

than the preceding background contribution, a strong cut is likely to be useful. However, once we impose the condition that at least two jets are b -like, the small mistagging probability ($\lesssim 10^{-3}$ for each of u, d, s, g [99]) ensures that this background is not of any importance.

- (iv) Semi-inclusive $b\bar{b} + n$ ($n > 1$) jets: Mainly QCD driven, the cross section is very large ($\sim 10^5$ pb) and depends crucially on the number of jets in the final state and on the minimum p_T (p_T^{\min}) allowed to the jets. Calculated using MADGRAPH, the cross sections have been validated against Refs. [100,101]. To this, we also add the contribution from $c\bar{c} + n$ ($n > 1$) jets, where the charm is mistagged as a b -jet.
- (v) Semi-inclusive VV production ($V = W/Z$): Diboson (WW, WZ and ZZ) production processes with a boosted gauge boson decaying hadronically can also mimic the fatjet signal. The cross sections for the aforementioned processes, at the NLO level, respectively are 119 pb, 47 pb and 16 pb [102].

For our analysis, though, we consider the semi-inclusive version with up to two extra jets, with the latter being required to satisfy $p_T(j) > 30$ GeV and $|\eta(j)| < 2.5$ and, in the case of two jets, $\Delta R(j, j) \geq 0.4$ as well. Considered at the LO level, using the 5 flavor scheme and MLM matching the corresponding cross sections are found to be ~ 120 pb, ~ 55 pb and ~ 16 pb respectively. As we would see later, these processes lead only to a minor component of the total background, mainly from WZ and ZZ events.

- (vi) Semi-inclusive HV production: Quite analogous to the previous set, these processes may contribute to the background for either signal channels, depending on whether the hadronic decays of Higgs or the W/Z boson are identified as the fatjet. The cross section for inclusive HZ process is ~ 1 pb and HW is ~ 1.8 pb at LO (when the cuts mentioned in the context of VV production above are imposed). While the higher order corrections can be found in Ref. [103] and the references therein, this contribution is subdominant even in the context of the $Hb\bar{b}$ mode.
- (vii) Single top production: Despite being semiweak processes, the total cross section ($\sigma_{tW} = 83.1$ pb, $\sigma_{tb} = 248$ pb and $\sigma_{tj} = 12.35$ pb at NNLO [104]) is quite comparable to the QCD-driven $t\bar{t}$ cross section, in a large part on account of the phase space. However, once the large p_T^{\min} criterion is imposed, the contribution is suppressed to a great degree.

As the kinematic distributions for the inclusive n -jet cross sections are somewhat similar to the inclusive $b\bar{b}$ events (both being largely QCD-driven), we, henceforth, merge the two and term it “inclusive $b\bar{b}$ ”. Of course, in doing this, tagging efficiency and/or mistagging probability

(as the case may be) are duly taken care of. Furthermore, we would subsume the relatively smaller contributions accruing from inclusive- VV, VH and single top events into an “others” category.

For the H -fatjet channel, some quantitative changes in the background profile turn out to be crucial. For example, with m_H varying significantly from m_Z , the fraction of the electroweak gauge bosons (whether emanating from hard $V + \text{jets}$ or hard $VV + X$ production or from the decay of tops), reconstructing as a H -fatjet reduces considerably. On the other hand, new processes such as inclusive H -production (whether QCD-initiated or as a result of vector-boson fusion) and Higgsstrahlung processes (WH, ZH or even $t\bar{t}H$) now need to be considered. Fortunately, the corresponding cross sections are much lower, especially for the event topology that we need to consider. Naively, this would already suggest that the Higgs-channel would be the more sensitive one.

C. Details of simulation

Implementing the model in FeynRules [105,106], we generate signal and background events at the tree order using MADGRAPH [107] interfaced with PYTHIAS [108] for parton showering and fragmentation. A given hard process contributing to either signal or background is generated with up to two additional partons to account for QCD radiations. To avoid possible inconsistencies (such as overcounting) arising from interfacing such matrix elements with parton showering algorithms, we employ the MLM matching scheme [109,110] with matching parameters as suggested in Refs. [111,112]. Signal events are simulated for mass points in the range $m_B \in [0.8, 3]$ TeV. The events are passed through DELPHES 3 [113], in order to implement detector effects and applying reconstruction algorithms. Jets are reconstructed using the anti- k_T algorithm [83] in FastJet [114], with $p_T > 30$ GeV and $R = 0.5(0.8)$. We impose $\Delta R(j, j) > 0.4$ and $|\eta| < 2.5$ on the jets. For other parameters, we use the default CMS card. To identify b -jets, we use a b -tagging module inside DELPHES, with the (p_T, η) -dependent tagging efficiency being in the 70–80% range. The probability of mistagging a charm as b -jet is 10% while for the other quarks and gluons, it is 0.1% or less. A lepton ℓ is considered to be visible and isolated only if it simultaneously satisfies $p_T > 10$ GeV, $|\eta| < 2.5$ and $\Delta R(\ell, j) > 0.4$ for all the jets in the event.

We implement jet substructure techniques to distinguish the fatjets from ordinary ones. The former are reconstructed and identified with the FastJet module demanding $p_T > 200$ GeV and $|\eta| < 2.4$. As for the radius parameter R , we investigate the performance for different values but, for brevity’s sake, present the result for only two choices. The first, namely, $R = 0.8$, is a more conventional choice and enables tracking down the decay products of Z even when the latter is not highly boosted. The second choice, *viz.*,

$R = 0.5$, is aimed toward reconstructing a heavily boosted Z . This is expected to be particularly useful for large m_B . For other parameters of the jet-substructure observables, as mentioned in Sec. III, we follow Ref. [65].

Since jet energy measurements are very crucial for our analysis, it is important to consider the energy resolutions, especially in the context of the hadronic calorimeter. This, however, depends on the particular detector being considered, and, furthermore on whether one is considering the barrel, endcap or the forward region [115,116]. Multiple sources (such as stochastic term, white noise *etc.*) contribute:

$$\frac{\sigma_E}{E} = \frac{a_s}{\sqrt{E/1 \text{ GeV}}} \oplus \frac{a_w}{E/1 \text{ GeV}} \oplus a_C,$$

with the terms to be added in quadrature. The constants $a_{s,w,C}$ depend on the details of the detector (and the geometric location within), and typically $a_s \in (0.5, 0.65)$, $a_C \in (0.03, 0.06)$ and $a_w \lesssim 5$. Similar expressions hold for the electromagnetic calorimeter as well, but with smaller a_i . However, since we are not interested in either photons or e^\pm , the resolution of the electromagnetic calorimeter is of little interest to us.

In addition, the granularity of the detectors implies a finite angular resolution. This, in principle, would be significant for the measurement of both the missing transverse momentum, and, more importantly, the invariant mass of a jet pair. However, in practice, these uncertainties are of little concern in view of the relatively large error in the jet energy measurements.

D. Signal and background profiles for different choices of R

With the profiles (both signal and backgrounds) for the two channels, *viz.*, Z or H , being quite similar, for the sake of brevity, we discuss only the former. This choice is also occasioned by the fact that this would turn out to be the one with the worse signal-to-background ratio.

Since the hard process corresponding to our signal comprises of a fatjet accompanied by another pair of b -tagged jets, we preselect events with a *minimum of three* relatively central ($|\eta| < 2.5$) jets, each with a minimum transverse momentum⁸ $p_T > 30$ GeV, demanding that they be separated by at least $\Delta R(j, j) > 0.4$. Arranging them in the descending order of p_T , as $j_0, j_1, j_2, j_3, \dots$, we display, in the top panel of Fig. 3, the p_T distributions of the leading (j_0), subleading (j_1) and subsubleading (j_2) jets for each of the three benchmark points. For a more massive B -quark, its decay products would be more energetic in its rest frame, resulting in a harder p_T spectrum. For the two leading jets, this is reflected by the top left and top center panels of Fig. 3. jets. The distribution for the subsubleading jet (top

right in Fig. 3) is a little more intricate. For most signal events, this jet would originate from the primary b (produced in association with the B). This explains the similarity in the three normalized spectra. It should also be realized that, as m_B grows large, it provides a scale for the kinematics, and a somewhat large $p_T(B) = p_T(\bar{b})$ would not cause significant suppression. This explains the slightly harder $p_T(j_2)$ spectrum for larger m_B .

While the decay of a very massive B would result in very energetic daughters, not all of the energy would be manifested in the form of transverse momenta. In view of this, we also investigate the energy of the three jets (as defined in the laboratory frame). Although such a variable is not very popular in the context of a hadronic collider (owing to the lack of information of the longitudinal momentum of the subprocess center-of-mass), we would find this to be useful. The middle panel of Fig. 3 exhibits the distribution in E_j for each of the three leading jets. Qualitatively, the features of the p_T distributions are replicated except that the spectra are hardened (understandably) and sharpened.

The relative hardness of the individual p_T spectra is also reflected (Fig. 3, bottom left) by that for $H_T (\equiv \sum_{\text{jets}} p_T)$, the scalar sum of the individual jet p_T s. Note, though, that the difference between those for the three benchmark plots is somewhat obscured by the inclusion of *all* jets in H_T , not just the leading three. Much the same story is repeated by the distribution in the sum of all jet energies (Fig. 3, bottom center). Another potentially interesting kinematic variable is the missing transverse energy (MET). In the present context, it could arise from two sources, the first being the neutrinos that result from leptonic decays, whether that of an entity involved in a hard process or from the hadrons in the cascade. A second, and given the large jet energies, often more important source is the mismeasurement of jet energies (as described in the preceding subsection). A third possible source is the event of a jet constituent not being registered in the detector, including the possibility of entities passing through detector gaps. Short of a full detector simulation, though, we cannot include the last-mentioned contribution. However, it is not expected to be a large effect. As we see in Fig. 3, the MET, typically, tends to be not too large (a consequence of there not being a hard invisible particle in the event) and its distribution has only a relatively small dependence on m_B .

We turn, now, to a discussion of the various contributions to the background. In Fig. 4, we display the corresponding kinematic distributions. The p_T and energy distributions for the backgrounds are much softer than those for the signal. This, of course, is expected as far as the two leading jets $j_{0,1}$ are concerned, simply on account of the large m_B that we are interested in. As far as j_2 is concerned, the relative hardness of the signal profile can be understood by realizing that it is m_B that provides the dominant scale in the production and a momenta of a few hundred GeVs does not exact too large a price. Consequently, harder cuts

⁸We impose a stronger p_T cut later on.

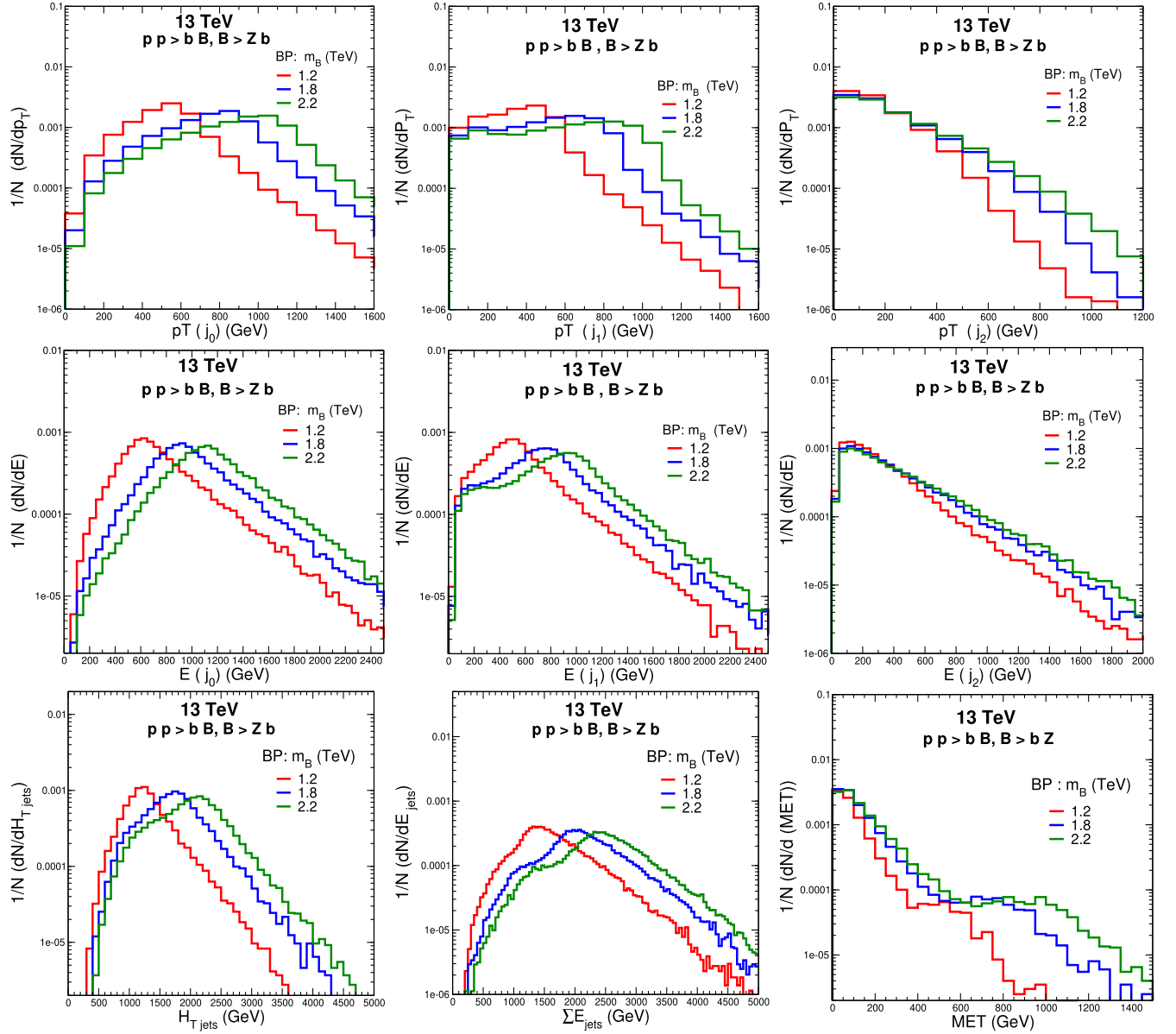


FIG. 3. Kinematic distributions for the signal with jets defined using a radius $R = 0.5$. Each of the three benchmark points are depicted. Top panel: p_T distributions for the three leading jets j_0 (left), j_1 (center) and j_2 (right). Middle panel: corresponding distributions for jet energy. Bottom panel: the scalar sum of the p_T s of all jets (left), the sum of all jet energies (center) and the missing transverse momentum (right).

on p_{Tj} or E_j are expected to improve the signal-to-background ratio. It should be realized, though, that the p_T distributions for inclusive $t\bar{t}$ production are relatively wider than those for the other backgrounds. This difference is even more stark for the H_T distribution and, thus, a cut on H_T would not preferentially remove this background over the signal. As this feature has its origin in the large number of jets resulting from inclusive $t\bar{t}$ production,⁹ it might seem

⁹Note that it is the hadronic decay of the top-pair that is of concern here, for a lepton veto would remove the bulk of the background from semileptonic decays.

that a restriction on the maximum number of hard jets might be useful in improving the signal-to-background ratio. This, however, is not a good option as, apart from the cut-definition sensitivity bringing into question the infrared safety, an inordinately large fraction would be lost from an already small signal size. Instead, a cut on H_T , augmented by a minimum requirement for $\sum_j E_j$ (see Fig. 4, lower center) would serve the purpose better. Also displayed, in the lower right panel, is the distribution in the MET for each of the individual contributions to the background. It can be easily ascertained that it is only the inclusive $t\bar{t}$ process that has an MET spectrum significantly harder than that for the

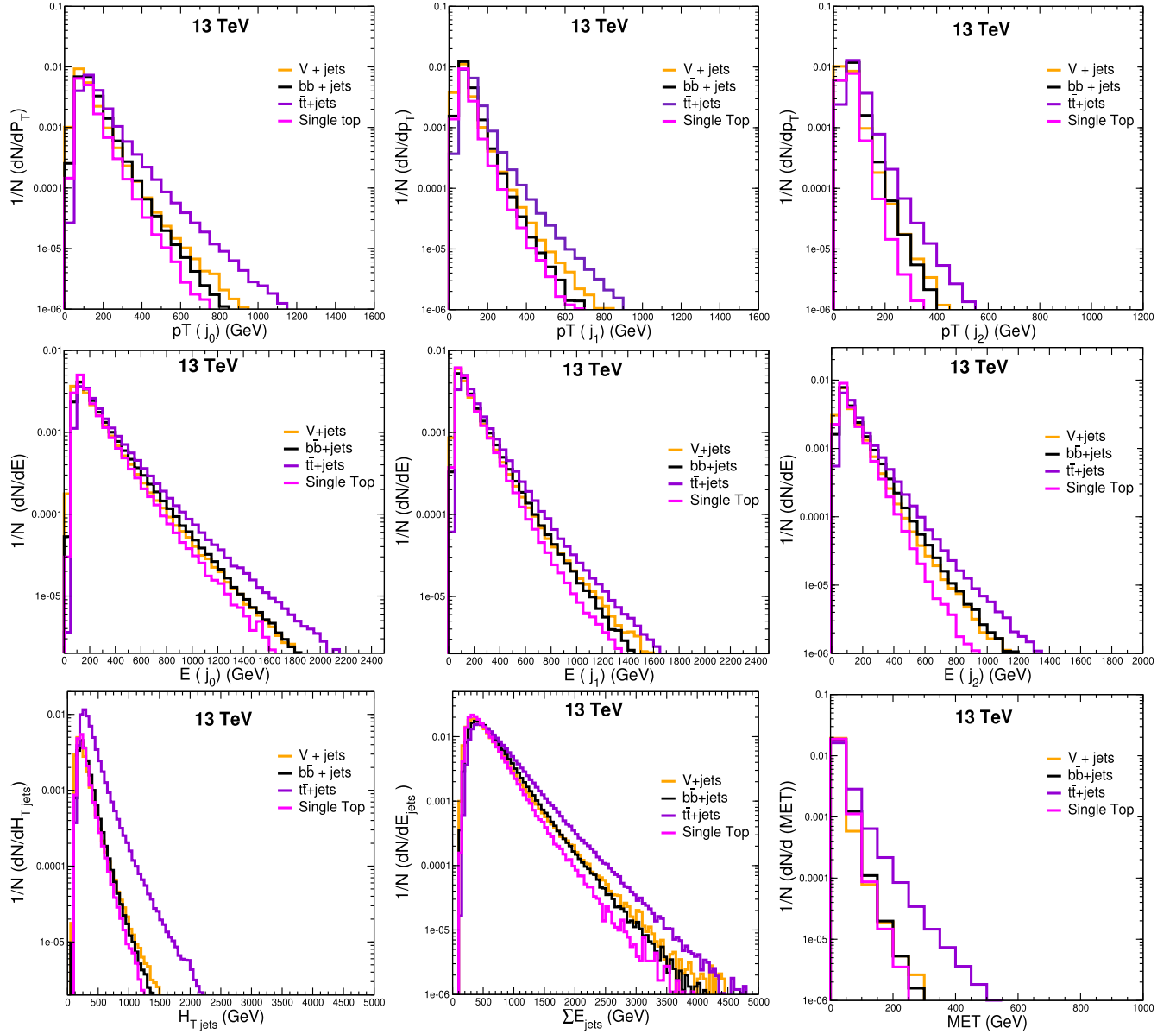


FIG. 4. Kinematic distributions for the major backgrounds with jets defined using a radius $R = 0.5$. Top panel: p_T distributions for the three leading jets j_0 (left), j_1 (center) and j_2 (right). Middle panel: corresponding distributions for jet energy. Bottom panel: the scalar sum of the p_T s of all jets (left), the sum of all jet energies (center) and the missing transverse momentum (right).

signal, the reason being attributable to both the possible presence of neutrinos in the former set of events as also the large number of jets, each with its associated energy resolution.

The analysis presented so far corresponds to a particular choice of the jet radius R used for jet reconstruction, namely $R = 0.5$. Had we chosen a somewhat different value, the aforementioned distributions would suffer only relatively small quantitative changes and no major qualitative ones. The rationale for our choice, as compared to the more canonical $R = 0.8$ would become manifest soon.

At this stage, we make our first identification of a fat Z -jet, selecting only those events that contain a jet, termed J_Z , that satisfies the twin conditions of¹⁰

$$m(J_Z) \in [80, 105] \text{ GeV}, \quad p_T(J_Z) > 200 \text{ GeV} \quad (12)$$

As the Z would need to be highly boosted for its daughters to coalesce into a single (fat) jet, the requirement on its p_T is not expected to lead to a significant loss of signal. Note

¹⁰The identification of a fat H -jet, appropriate for the other channel, proceeds analogously, with $m(J_H) \in [110, 140] \text{ GeV}$.

TABLE I. The fraction of events where one of the three leading jets can be identified as fatjet with $p_T > 200$ GeV. Jets are reconstructed with a radius $R = 0.5$ with the parenthetical numbers denoting results for $R = 0.8$.

Signal events				
m_B (TeV)	% of j_0	% of j_1	% of j_2	Total (%)
1.2	24.5(28.8)	9.2(14.4)	1.2(3.0)	34.9(46.2)
1.8	30.8(30.8)	12.8(15.4)	1.5(3.0)	45.2(49.3)
2.2	32.8(31.3)	13.3(15.5)	1.5(2.9)	47.7(49.8)
Background events				
Process	% of j_0	% of j_1	% of j_2	Total (%)
$V + \text{jets}$	0.1(0.6)	0.02(0.17)	0(0)	0.13(0.78)
$b\bar{b} + \text{jets}$	0.1(0.82)	0.02(0.24)	0(0.01)	0.13(1.08)
$t\bar{t} + \text{jets}$	1.36(6.72)	0.28(1.9)	0.01(0.17)	1.66(8.81)
Single top	0.16(1.33)	0.05(0.52)	0.0(0.02)	0.22(1.87)
Di-boson	0.93(3.72)	0.26(1.11)	0.02(0.04)	1.22(4.88)

that, even for the signal, not all events would contain such a jet. For one, some of the putative Z -jets could merge with other jets (or incorporate hadrons with a different origin), thereby augmenting its mass to beyond 105 GeV. Similarly, some of its constituents may go missing in the jet reconstruction algorithm. Finally, there is the probability of a jet energy mismeasurement. As Table I shows, only in 35%–50% of the signal events, is a Z actually reconstructed as a fatjet. Fortunately, though, the probability of reconstruction is much smaller for the background events (see Table I). This suppression is, understandably, extreme for the potentially largest contributors to the background, namely inclusive¹¹ $b\bar{b}$ and QCD n -jets, as there are no gauge-bosons in such events. The large suppression for the $t\bar{t}$ and diboson backgrounds owes itself to two factors. For one, the top-production events have only W 's and not a Z , whereas, of the diboson events, only a fraction have Z 's. Second, a relatively small fraction of these gauge bosons have a p_T sufficiently large for the daughter to coalesce into a fatjet defined using $R = 0.8$. For our favored choice, namely $R = 0.5$, this fraction is smaller still.

It is also instructive to examine the distribution of the fatjet within the three leading jets. As for the signal events, *a priori*, one would imagine that, the Z is as likely to lead to j_1 as compared to j_0 . While this is indeed true, the differing rates in Table I can be understood by realizing that if J_Z is to be identified with j_1 , it would require that j_0 must have a p_T substantially larger than 200 GeV. Naturally, only a smaller fraction of events would satisfy this. Similar arguments also explain the much fewer incidences of j_2 (or, $j_{3,4}$ etc., if the exist) being identified as the fatjet.

Particularly important, in this analysis, is our choice of the jet radius R . With the gauge bosons from such background events not being highly boosted, the choice $R = 0.5$ implies that the daughters of the gauge boson are more likely to be reconstructed as two independent jets rather

than a single fatjet. This has to be contrasted with the case of the signal where the Z tends to be highly boosted. Sure enough, an increase to $R = 0.8$ would significantly enhance the probability for background as opposed to a very small increase for the signal events (see Table I). This vindicates our use of $R = 0.5$.

In Fig. 5, we display a few kinematic distributions of importance constructed for events that do contain a fatjet as defined by Eq. (12). Even a cursory comparison of the two leftmost panels establishes that a much stronger restriction on the J_Z transverse momentum, such as $p_T(J_Z) > 400(500)$ GeV would significantly reduce the background without impinging much on the signal strength. Also shown in Fig. 5 are ratios of the missing transverse momentum MET with H_T (central panels) and the p_T of the leading b -tagged jet. Despite the former having remarkably different structure for the signal and backgrounds, a restriction on this ratio so as to enhance the signal-to-background ratio would, simultaneously, reduce the total size of the signal drastically. On the other hand, the ratio MET/p_T would turn out to be an useful discriminant.

Once the fatjet J_Z has been identified in the correct mass window, we consider, next, the two hardest of the remaining jets. The one with the maximal azimuthal separation with J_Z is christened J_1 and the other as J_2 . This identification is particularly useful in identifying the signal events. With the very heavy B , typically being produced with a relatively small transverse momentum, *viz.* $p_T(B) \ll m_B$, its daughters (J_Z and the putative J_1) are likely to be produced with $\Delta\phi(J_Z, J_1) \sim \pi$, as is seen in Fig. 6 (left). Consequently, the corresponding ΔR too tends to be large as in Fig. 6 (right). Such a strong preference is not expected of the background events. That $\Delta\phi(J_Z, J_2)$ has a slight preference for large values as well is understandable, for the \bar{b} produced along with the B would have a small momentum too; consequently, momentum conservation would stipulate that the transverse component would prefer to be opposite that of the leading transverse momentum in the event, namely that of

¹¹Note that we have not yet imposed b -tagging requirement.

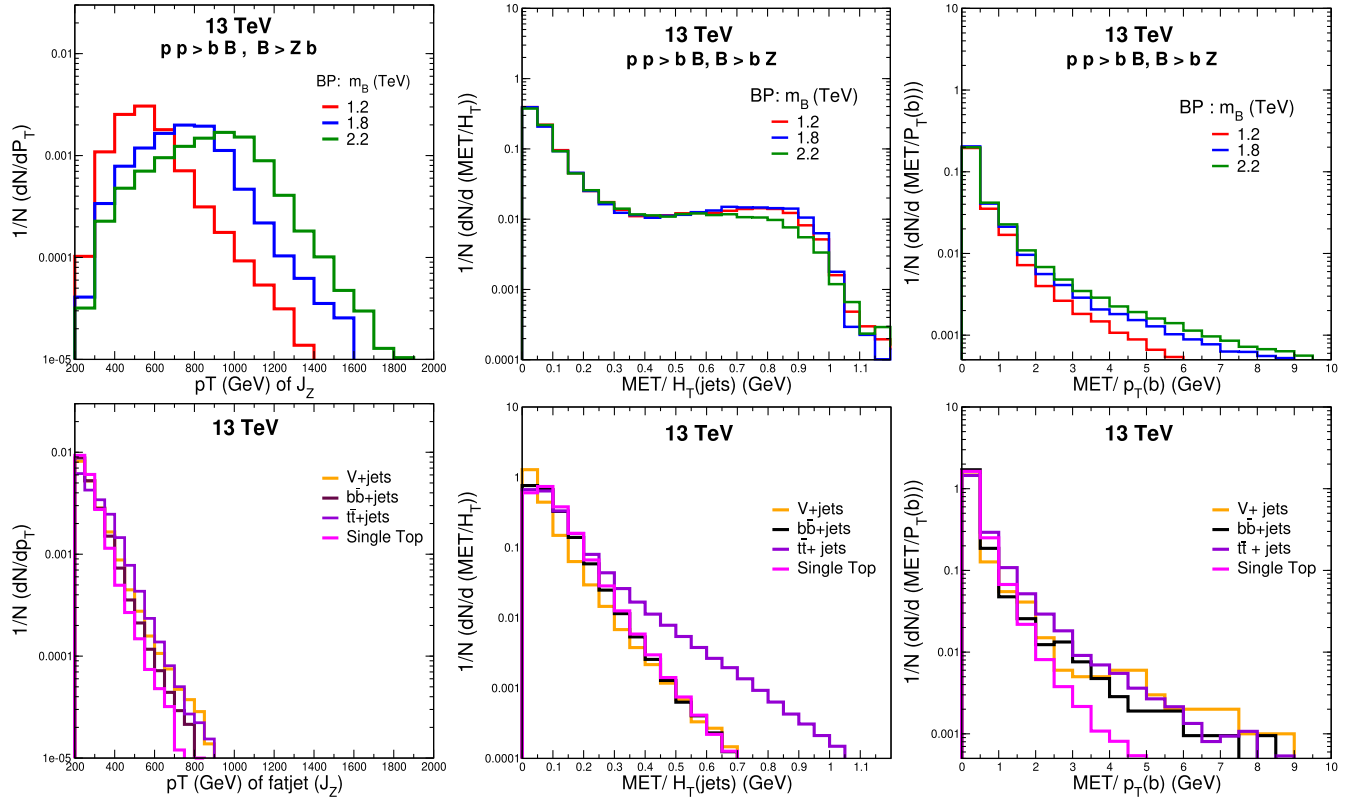


FIG. 5. Kinematic distributions after demanding the existence of a Z -fatjet (where jets are reconstructed with $R = 0.5$) with $p_T(J_Z) > 200$ GeV and $m(J_Z) \in [80, 105]$ GeV.

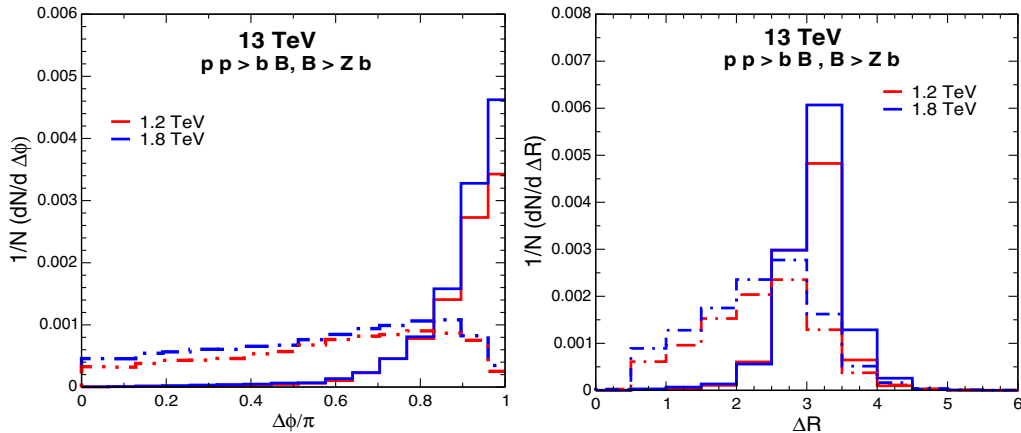


FIG. 6. Left: solid (dashed) curves show the distribution in azimuthal distance between J_Z and $J_1(J_2)$ for two signal BPs. Right: analogous distributions for ΔR . The fatjet J_Z are required to have $p_T > 200$ GeV and jetmass in the $[80, 105]$ GeV range. The basic cuts as mentioned in Sec. 4.3 are imposed too.

J_Z . It might seem, though, that analogous arguments would hold for the backgrounds too. This is only partially true though, for some of the contributions tend to have a larger sphericity. And, finally, in the event of multijet events, we find that the probability of the true b -daughter of the decaying B not leading to J_1 is much less than 1%, thereby establishing the robustness of the identification.

This contention is further supported by Fig. 7 where we display the two body (J_Z and J_1) invariant mass distribution, for different signal BP's as well as individual backgrounds. With the background falling away at large values of this invariant mass, we expect that restricting ourselves to $|m_{\text{inv}} - m_B| \leq 3\Gamma_B$ would further accentuate the sensitivity for large m_B (a region with small signal cross sections).

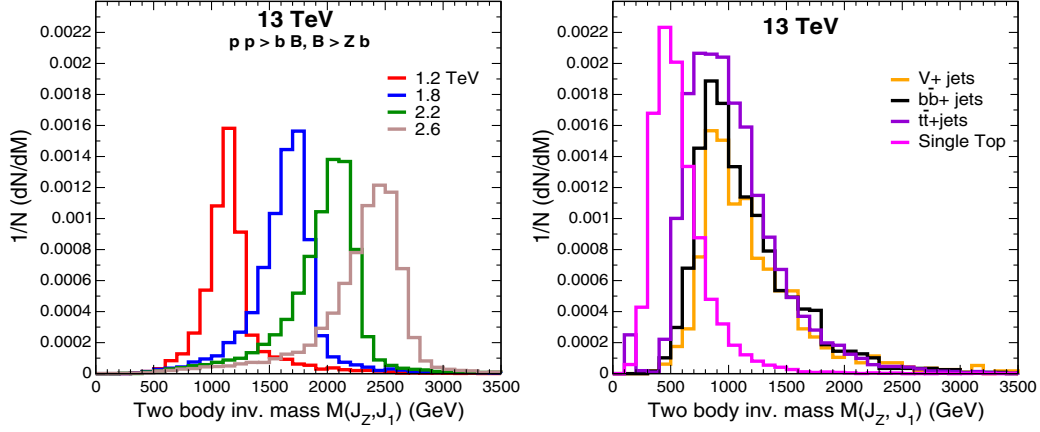


FIG. 7. The distribution in the two body invariant mass of the fatjet J_Z and J_1 for the signal (left) at different BP's and the major background (right). Fatjets are selected with $p_T > 200$ GeV and jetmass within $[80, 105]$ GeV, using $R = 0.5$. The basic cuts as mentioned in Sec. 4.3 are imposed.

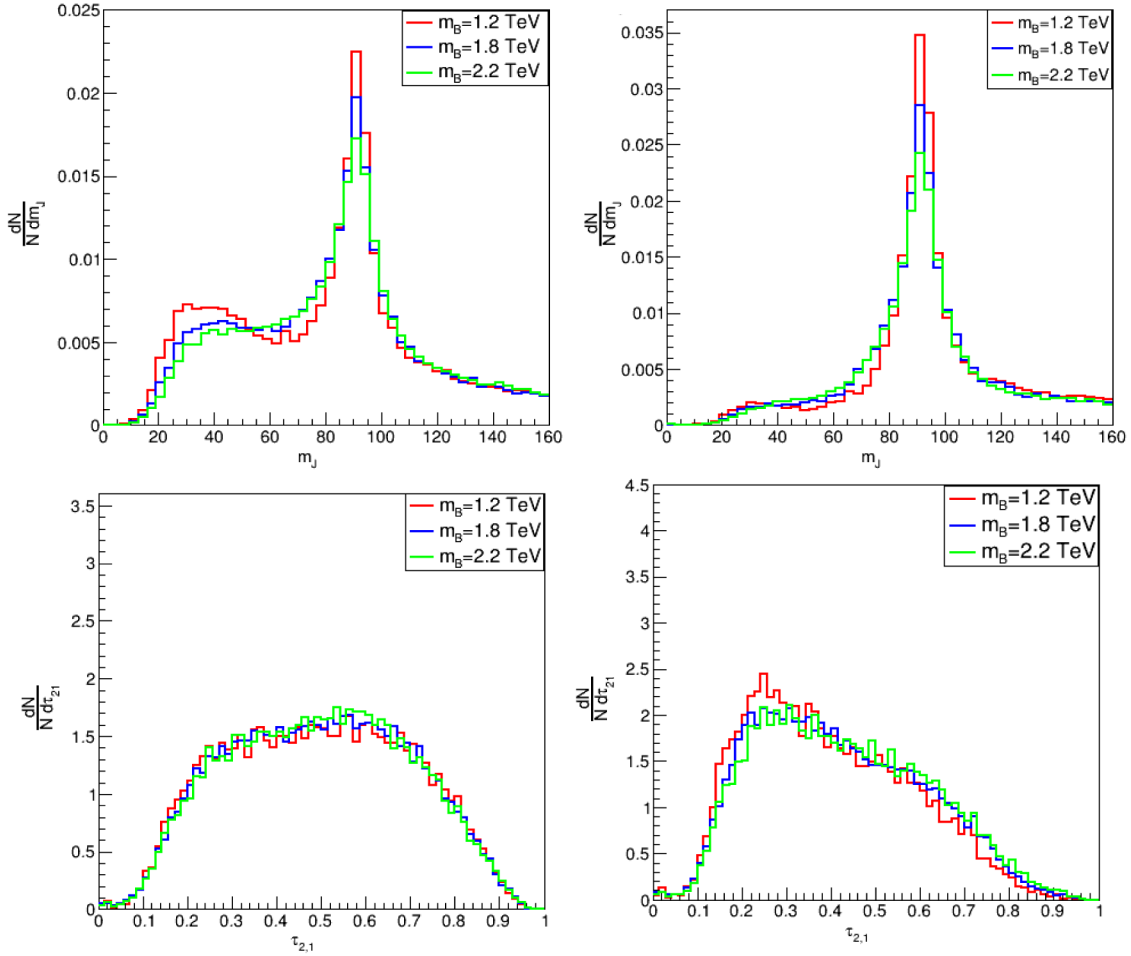


FIG. 8. The jet mass (m_J) and τ_{21} distributions for a fatjet (of $p_T > 500$) as constructed with a radius parameter $R = 0.8$ and Top: distributions of m_J before any τ_{21} cut (left) and after $\tau_{21} < 0.5$ (right) for three signal BP's. Bottom: distributions in τ_{21} before any cut on m_J (left), after a cut of $80 < m_J < 105$ GeV (right).

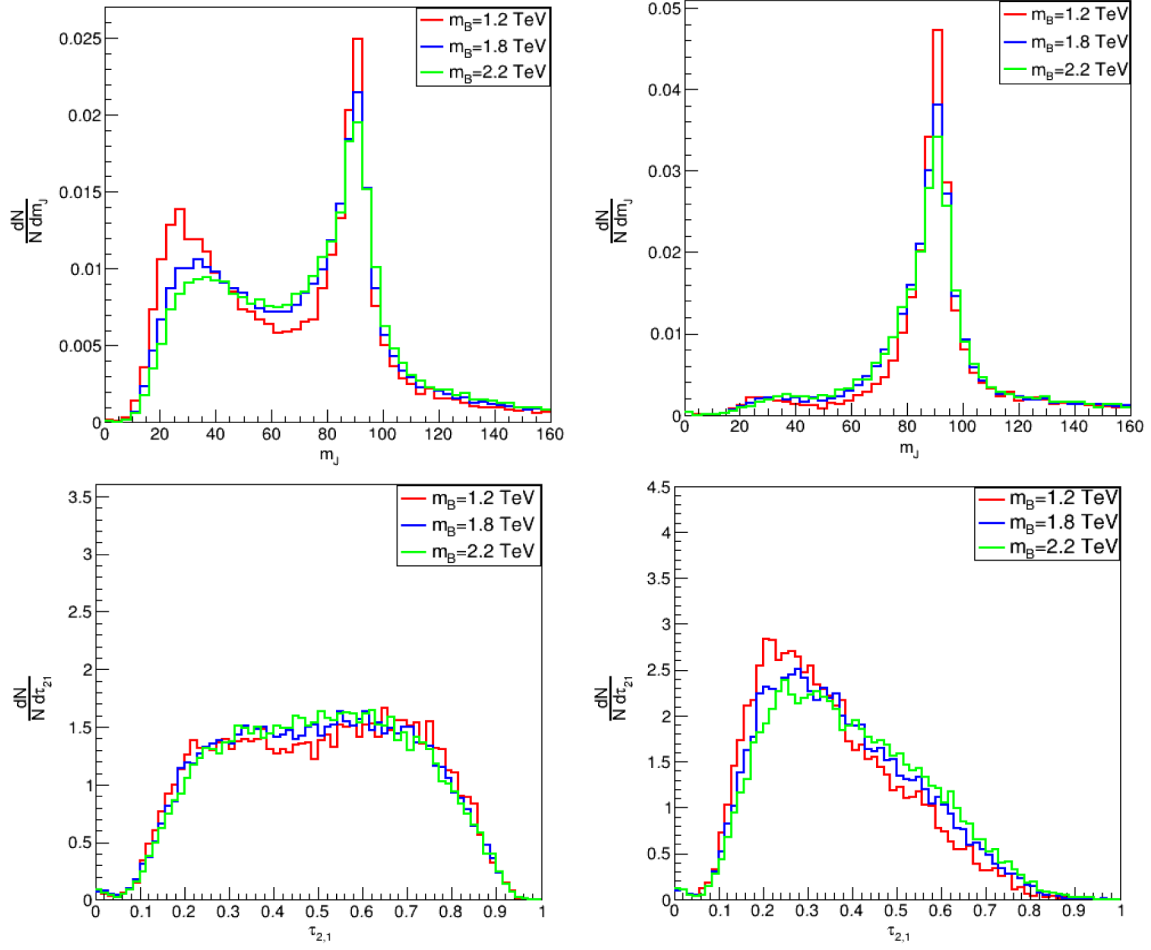


FIG. 9. The jet mass (m_J) and τ_{21} distributions for a fatjet (of $p_T > 500$) as constructed with a radius parameter $R = 0.5$ and Top: distributions of m_J before any τ_{21} cut (left) and after $\tau_{21} < 0.4$ (right) for two signal BP's. Bottom: distributions in τ_{21} before any cut on m_J (left), after a cut of $80 < m_J < 105$ GeV (right).

E. Fatjet characteristics for signal and background

In the preceding subsection, we have demonstrated the importance of demanding a fatjet (J_Z) in the signal. The criteria to define a jet to be a fat one, though, were *ad hoc* in nature. We, now, reexamine such issues, aiming to best define it. To this end, we take a few steps back, not only relaxing the criteria on the fatjet mass (as described in the preceding subsection), but also reconsidering the radius R used to define jets.

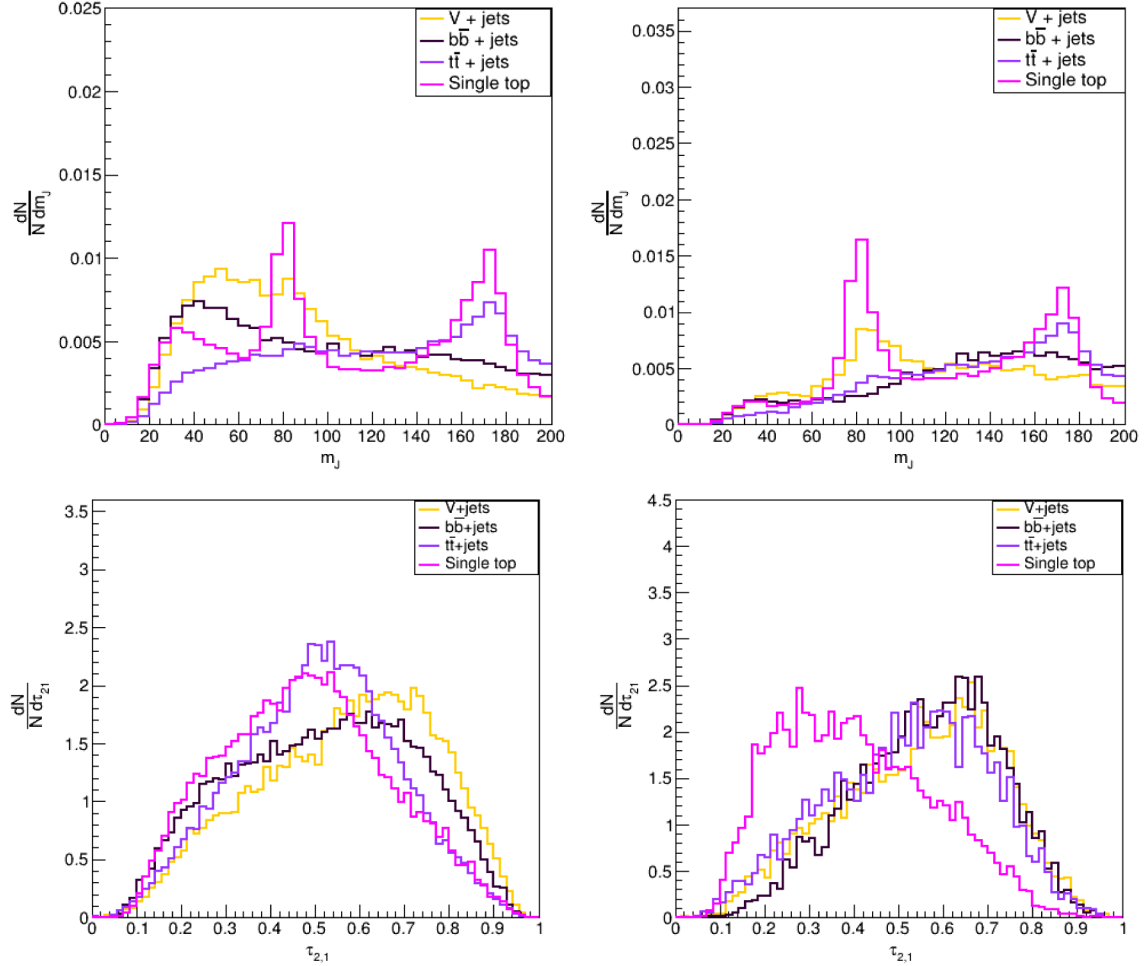
To begin with, we consider the popular choice of $R = 0.8$. In Fig. 8, we display two important characteristics of the putative fatjet, requiring it only to satisfy $p_T > 500$ GeV. The left panels show the distributions without any further cuts, the top one for the jet mass, and the bottom one for the ratio of two subjeettiness parameters [see Eq. (10)], *viz.*, $\tau_{21} \equiv \tau_2/\tau_1$. While there exists a peak at m_Z , there is a hint of a second peak a little below 40 GeV. The latter can be understood in terms of relatively hard and asymmetric QCD radiations. The expectation value of the mass of such jets (calculated, for example, by considering the $q \rightarrow qg$

splitting function and then performing the θ and z integrations) is given by [117]

$$\langle m^2 \rangle = \frac{3\alpha_s}{8\pi} C_F p_T^2 R^2 \quad (13)$$

and, hence, the mass scales linearly with jet p_T and the radius parameter R . That the low-energy peaks in Fig. 8 are indeed QCD-driven is also attested to by the gradual drop around the central value [117], as distinct from sharp peak corresponding to an on-shell particle decay. Such an origin also explains why the peak is more pronounced for smaller m_B . Notwithstanding our ability to explain the secondary peak, its very presence and size seems to argue against the identification of the fatjet as a two-pronged decay. Similarly, the τ_{21} distribution does not show any inclination for $\tau_{21} < 0.5$, as a two-prong system should, ideally, favor.

It is interesting to consider, at this stage, the situation for jet reconstruction using $R = 0.5$, as detailed in Fig. 9. The aforementioned secondary peak (at $m_J \lesssim 40$ GeV) is even more pronounced now, thanks to the fact that such an R


 FIG. 10. As in Fig. 8, but for the leading contributions to the background with $R = 0.8$.

calls for narrower jets. Quite analogously, the preference for $\tau_{21} > 0.5$ is strengthened. Both these arguments would seem to call for $R = 0.8$ being a better choice. This is, however, belied by an examination of the right panels for both Figs. 8 and 9. The top right panels in both clearly demonstrate that a cut¹² on τ_{21} strongly accentuates the Z -peak, simultaneously obliterating the secondary peak at low m_J . Analogously, requiring the jet mass to lie in the $80 \text{ GeV} \leq m_J \leq 105 \text{ GeV}$ window results in the τ_{21} distribution showing a clear bias for $\tau_{21} < 0.5$ (bottom right panels). Both these observations are as expected, for it is only such events that should show up as two-prong decays of the Z . Indeed, were we to consider a two-dimensional distribution (in the τ_{21} - m_J plane), the event rate would show a clear correlation between these two kinematic variables.

It is interesting to note that the τ_{21} distribution, after effecting the fatjet mass window restriction, is slightly

¹²The differing choices for this cut (for the two values of R) is occasioned by consideration of optimizing the signal-to-noise ratio.

flatter for a larger m_B . This holds true for both choices of R (see Figs. 8 and 9) and is but a consequence of the fact that as the fatjet is boosted more and more, the distinction between one-prong and two-prong configurations is progressively blurred. This can be understood by examining the Z decay into a $q\bar{q}$ pair which, through their subsequent radiation, putatively lead to the two smaller cones within the fatjet. In calculating τ_2 [see Eq. (10)] two subjet axes are assigned along the direction of these two cones. For an individual fatjet constituent, the minimum of the two ΔR s between the constituent and the assigned axes contributes to τ_2 . Consequently, the value of τ_2 tends to be small. On the other hand, in calculating τ_1 , only one subjet axis is defined and assigned along the direction of the fatjet. Consequently τ_1 for $m_B = 1.8 \text{ TeV}$ is smaller than that for $m_B = 1.2 \text{ TeV}$ resulting in a flatter τ_{21} distribution for the former case.

It should be further noticed that the τ_{21} distribution is sharper in Fig. 9 compared to Fig. 8. Again, this was to be expected given that a smaller value of R will allow for smaller amount of secondary radiations within the cone. As we shall shortly see, the situation is markedly different for

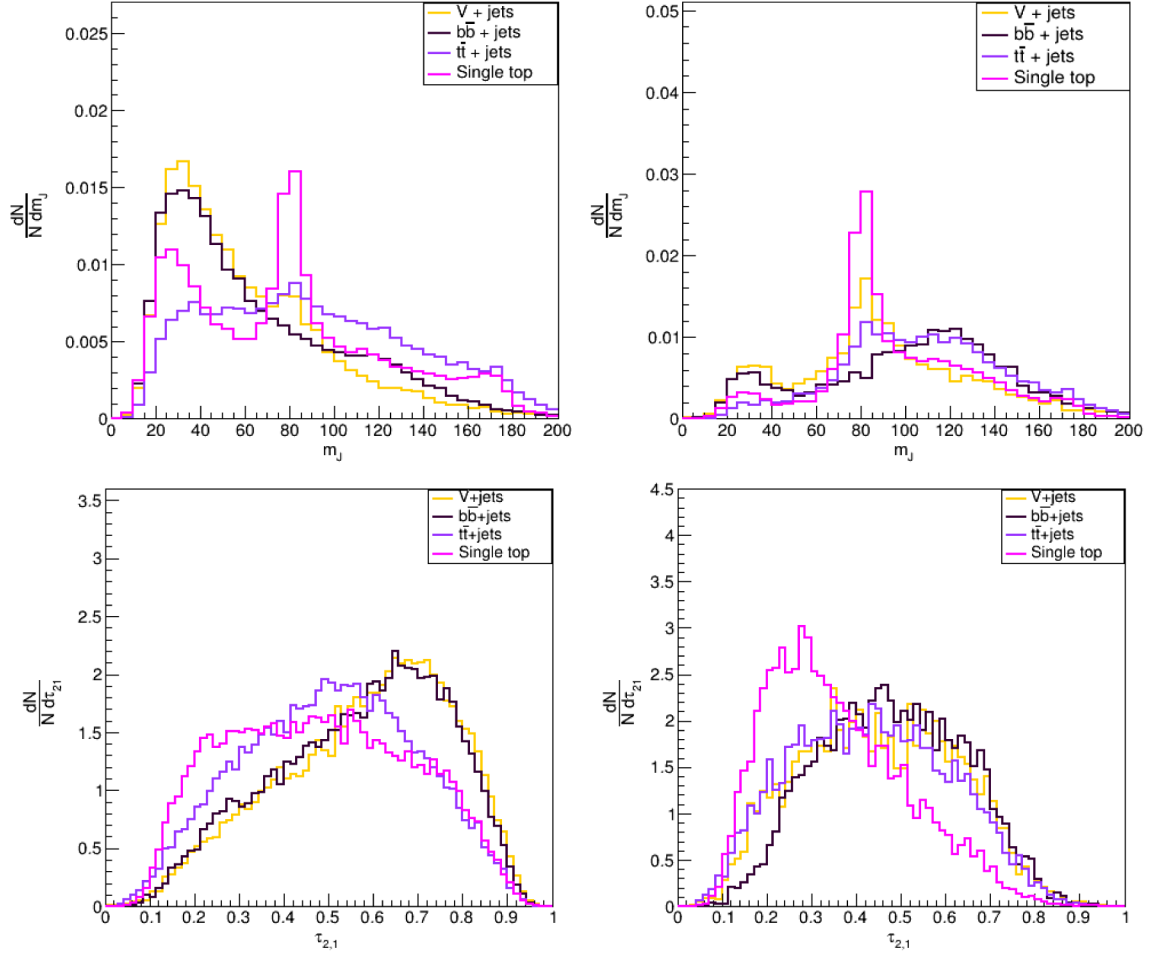


FIG. 11. As in Fig. 9, but for the leading contributions to the background with $R = 0.5$.

the top-decays contributing to the background and, together, this prompts us to adopt $R = 0.5$ as the definitive requirement. As for the jet-mass requirement, clearly the choice $[80, 105]$ GeV would be better than, say the $[65, 105]$ GeV one (as adopted in various analyses, on account of the former discriminating against W -backgrounds (whether from direct W production or from top-decays). Finally, we find the $p_T > 500$ GeV requirement to be a nearly optimal one.

We, now, consider the corresponding fatjet characteristics for the leading contributions to the background, once again for both $R = 0.8$ (Fig. 10) and $R = 0.5$ (Fig. 11). Concentrating on the top-left panel of Fig. 10, both the $t\bar{t}$ and the single-top contribution clearly show a peak at Fig. 10. The latter, in addition, shows a stronger peak close to the gauge boson masses. While, naively, one would also have expected the $t\bar{t}$ events to also show the second peak, courtesy the W in the decay chain, note that the large p_T demanded of the fatjet would mean that the W and the b would tend to coalesce into a single jet. The use of $R = 0.5$, instead, altogether removes the peak at $m_J \approx m_t$ (see Fig. 11). This can be understood by realizing that the

radius parameter is essentially set by $R \sim m_J/E_J$. For $R = 0.8$, the large p_T that has been demanded of the top (putative fatjet) allows it to decay within R ; and once the three prong nature of the top is resolved, it is identified as a fatjet. For the reconstruction of t -quark (as a fatjet) within a smaller radius of $R = 0.5$, a much higher energy is required of the top and only a small fraction of events would satisfy this. Rather, the fraction of events with m_J close to $m_{W,Z}$ is enhanced. Once again, the strong peaks at small m_J can be understood in terms of the secondary QCD radiation [see discussion surrounding Eq. (13)]. It is interesting to note that neither of the two aforementioned plots shows a peak at $m_J \approx m_t$ for the inclusive $t\bar{t}$ events. This can be understood by realizing that only a small fraction of such events would boast of a top with a p_T sufficiently large enough for the top to be manifested as a fatjet.

In the bottom panels of both Fig. 10 and Fig. 11, we plot the distributions of $\tau_{2,1}$ before any m_J cut (left) and after requiring $m_J \in [80, 105]$ GeV (right). Before the cut, none of the contributors to the background show a preference for $\tau_{2,1} < 0.5$. Even on imposition of the cut, it is only the single-top production that exhibits this

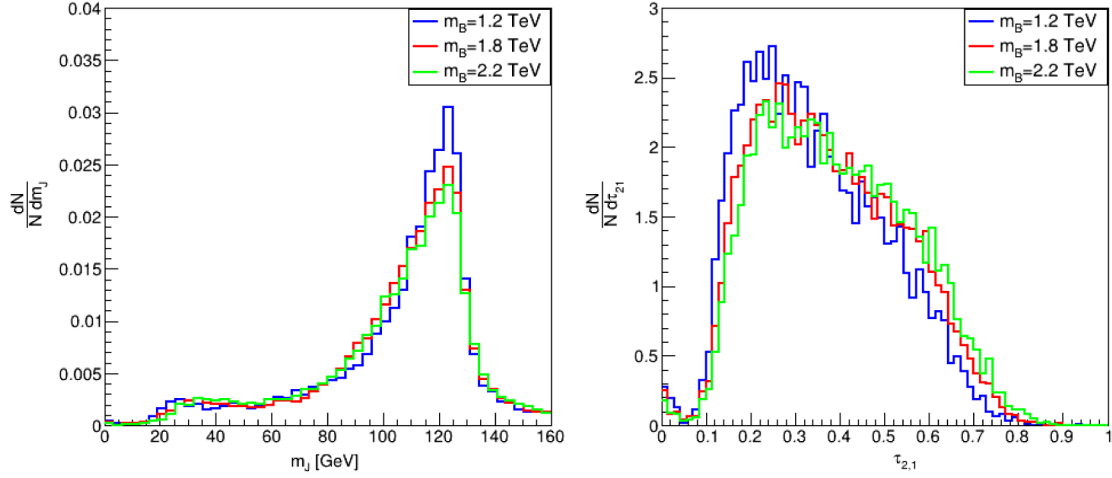


FIG. 12. Plots for Higgs-fatjet scenario, left one is jet-mass plot for $\tau_{21} < 0.4$ and the right one is τ_{21} plot after a mass-cut of $110 < m_j < 140$ with $R = 0.5$.

preference, primarily on account of the W . Similarly, for the $V + \text{jets}$ contribution, the m_j cut better accentuates the two-prong nature for $R = 0.5$ (than for $R = 0.8$). An analogous enhancement does not occur for the $t\bar{t}$ background (especially for $R = 0.8$) as a large fraction of the fatjet reconstruction, before the cut, would be associated with the entire top. The QCD jets being a diffuse spray of large angle radiation, the τ_{21} distribution for the inclusive $b\bar{b}$ events is, understandably, quite flat.

It might seem surprising that the top left panels of both Fig. 10 and Fig. 11 do not show a peak in the $m_j \in [80, 105]$ GeV for the $V + \text{jets}$ background. This can be understood by realizing that the gauge boson, very often, has a slightly smaller p_T than the leading QCD jet(s). Furthermore, the secondary radiation off the leading parton often leads to these being identified as the fatjet, especially when a strong cut is applied on the fatjet p_T . Consequently, the peak is smeared to a great extent. When the τ_{21} restriction is applied, the peak duly stands out.

With the event topology for bH being similar to bZ , and given that the difference $m_H - m_Z \ll m_B$, we would expect the Higgs too to lead to a fatjet. So, in Fig 12, we present the jet mass and the τ_{21} plots for the choice $R = 0.5$ for the Higgs scenario after putting a cut of $\tau_{21} < 0.4$ on the former and a cut of $110 < m_j < 140$ on the later. We see that the Higgs-mass and the two-prong behavior are correctly identified. A comparison of the results for the choices $R = 0.5$ and $R = 0.8$ leads us to conclusions similar to those reached for the Z -fatjet case with the τ_{21} distribution for $R = 0.8$ being flatter than the $R = 0.5$ case in the Higgs fatjet mass window. It is also evident from the background plots (left figures of Fig. 10) that in the jet mass region of $[110-140]$ the backgrounds are expected to be much smaller. The rest of the behavior of the backgrounds remain same and, hence, we do not show them separately.

F. Result

We begin by discussing the Z -fatjet channel in detail. The analysis for the H -fatjet channel (presented thereafter) follows analogously with some subtle differences, which would be highlighted. Thereafter, we delineate the part of the parameter space that could be ruled out by either channel or even lead to a discovery.

1. The Z -fatjet channel

As we have already discussed, the $R = 0.5$ choice is not only more commensurate with the two-prong nature of the signal, while suppressing the contributions from the $t\bar{t}$ background, but also allows for the imposition of a stronger cut on τ_{21} , so as to further reduce the backgrounds. Consequently, we would largely concentrate on this choice, and comment only briefly on the results for $R = 0.8$. Guided by the kinematic distributions for the signal and background events, as described earlier, we now discuss the selection cuts, in the order these are imposed, along with the effects these have.

- (i) Selection 1 (S_1): We require at least three jets, imposing a veto on isolated leptons satisfying

$$p_T > 10 \text{ GeV}, \quad |\eta| < 2.5, \quad \text{and} \quad \Delta R_{\ell j} > 0.4. \quad (14)$$

Ordering them according to the transverse momenta, the three leading jets must not only satisfy

$$\begin{aligned} p_T(j_0) &> 400 \text{ GeV}, & p_T(j_1) &> 250 \text{ GeV}, \\ p_T(j_2) &> 50 \text{ GeV} \end{aligned} \quad (15)$$

but also marginally stronger requirements on their total energy (in the laboratory-fixed frame), namely

$$\begin{aligned} E(j_0) > 500 \text{ GeV}, & \quad E(j_1) > 300 \text{ GeV}, \\ E(j_2) > 100 \text{ GeV}. & \end{aligned} \quad (16)$$

In addition, we require that

$$H_{T_{\text{jets}}} > 1000 \text{ GeV} \quad \text{and} \quad \sum_{\text{jets}} E > 1200 \text{ GeV}. \quad (17)$$

- (ii) Selection 2 (S_2): We require that at least one of the jets from the preceding stage gets resolved into a fatjet J_Z satisfying

$$m_J \in [80, 105] \text{ GeV} \quad \text{and} \quad p_T(J_Z) > 500 \text{ GeV} \quad (18)$$

Of the remaining jets (from among $j_{0,1,2}$), we name the one with the maximal azimuthal separation with J_Z as J_1 and demand that

$$\Delta\phi(J_Z, J_1) > 2.5. \quad (19)$$

- (iii) Selection 3 (S_3): Of the jets that have *not* been identified as a fatjet, we demand that at least two be b -tagged. In other words, we consider the semi-inclusive final state $N_b \geq 2$ (where we do not make any demand on the identity of the others). In addition, we demand that the ratio of the MET and the p_T of the leading b -jet be less than unity.
- (iv) Selection 4 (S_4): At this stage, we optimize the fatjet characteristics by effecting a single *fatjet selection* in terms of τ_{21} . We consider two choices, namely

$$(a)\tau_{21} < 0.5 \quad \text{or} \quad (b)\tau_{21} < 0.4. \quad (20)$$

The devolution of the signal cross section, as the selection criteria are applied consecutively, are summarized in Table II. The corresponding numbers for the backgrounds are presented too.¹³ As even a cursory comparison of these tables with the cross sections discussed in Sec. IV B shows, S_1 itself results in a severe preferential suppression of the background as compared to the signal. The subsequent imposition of S_2 retains $\sim 45\text{--}70\%$ of the signal events, while rejecting nearly 90% of the total background¹⁴ that survives S_1 .

As is evident from the tables, the signal-to-background ratio improves significantly once $N_b \geq 2$ is demanded, with the improvement being driven by that in the major channel, namely QCD-driven inclusive- $b\bar{b}$ production. This can be understood by realizing that the additional jets in such processes would often appear close to one of the b - or \bar{b} -induced ones and, together, would constitute the fatjet

¹³A caveat needs to be entered here. Keeping the S_3 selection in mind, we deliberately omitted, from the table, the multijet QCD events where the final state does not contain either of a $b\bar{b}$ or a $c\bar{c}$ pair. As argued earlier, such backgrounds are too small to be of any consequence here.

¹⁴It is obvious, though, that the suppression works differently for the individual contributions to the background.

TABLE II. Top: the variation of the cross section for the Z -fatjet signal ($B \rightarrow bZ$) in (fb), for each of the BPs, as subsequent selection cuts are imposed for LHC operating at $\sqrt{s} = 13$ TeV. We use $\kappa = 0.5$ and $R = 0.5$. Bottom: the corresponding variation for the various contributions to the background.

m_B (TeV)	S_1	S_2	S_3	$S_4(a)$	$S_4(b)$
1.2	122.1	56.25	24.14	19.32	16.9
1.8	15.5	10.52	3.89	3.1	2.7
2.2	4.1	2.9	0.98	0.74	0.64
Backgrounds	S_1	S_2	S_3	$S_4(a)$	$S_4(b)$
$b\bar{b} + \text{jets}$	3.45×10^4	4.68×10^3	560	283	140
$V + \text{jets}$	7.5×10^3	829	294	141	97
$t\bar{t} + \text{jets}$	2.97×10^3	973	433	325	238
<i>Others</i>	356	92	9.0	7.4	6.2
Total	4.53×10^4	6.57×10^3	1.3×10^3	737	481

(thereby leaving only one b -tagged jet among the rest). It should be pointed out at this stage that the remaining component of S_3 , namely $\text{MET}/p_T \leq 1$ for the leading b -tagged jet, is particularly effective in reducing the background contributions. A relatively large value of this ratio, especially for the inclusive $t\bar{t}$ production background, has two primary sources. For one, such processes are associated with multiple jets, with the associated MET accruing primarily from jet-energy mismeasurements. As for the events associated with semileptonic decays of the top, note that if the associated lepton be the electron or the muon, then an event with a large p_T carried by the neutrino would, most likely, be eliminated by the isolated lepton veto. This, however, does not hold for the tau-events, primarily because of the large semileptonic branching fraction for the latter and also because the leptonic decays tend to leave smaller momenta for the ensuing electron/muon. Thus, such events account for a large fraction of the high-MET background events.

As for selection S_4 , since it pertains only to the fatjet, it is naturally independent of the value of N_b . Furthermore, the alternative (a) is, understandably, less restrictive as compared to (b). As can be seen from a comparison of the two units of Table II, imposing $S_4(a)$ would retain roughly $\sim 53\%$ of the total background, but as much as $70\text{--}80\%$ of the signal (depending on m_B). The corresponding numbers for $S_4(b)$ are $\sim 33\%$ and $64\text{--}70\%$ respectively. The somewhat larger improvement due to $S_4(b)$ can be traced to the fact that the stronger τ_{21} cut is better able to selectively choose the two-prong fatjets. While a still stronger cut would further improve the signal-to-background ratio, it would be at the cost of signal strength and the consequent loss in the significance. Indeed, $S_4(b)$ represents a near-optimal choice. To understand the differing strength of $S_4(a, b)$ when applied to the different contributions to the background, we draw attention to

TABLE III. The signal and total background cross section after S_3 and $S_4(b)$ in the $|m(J_Z, J_1) - m_B| \leq 3\Gamma_B$ bin for $\kappa = 0.5$ is presented for the Z -fatjet signal ($B \rightarrow bZ$). The comparison among the significances(σ), evaluated at 300 fb^{-1} is also shown for b -jet ≥ 2 . We also quote the significance(σ), evaluated at 300 fb^{-1} for $R = 0.8$ for comparison.

$R = 0.5, b\text{-jet} \geq 2$		After S_3			After $S_4(b)$		
$m_B \pm 3\Gamma_B$ (TeV)	$1.2 \pm 3\Gamma$	$1.8 \pm 3\Gamma$	$2.2 \pm 3\Gamma$	$1.2 \pm 3\Gamma$	$1.8 \pm 3\Gamma$	$2.2 \pm 3\Gamma$	
Signal (fb)	11.34	2.11	0.55	7.94	1.47	0.36	
Background (fb)	146.2	41.8	22.0	60.8	18.0	9.1	
Significance (σ_{300})	16.25	5.63	2.03	17.63	6.02	2.05	
$R = 0.8, b\text{-jet} \geq 2$		After S_3			After $S_4(b)$		
Significance (σ_{300})	10.3	1.6	0.9	9.4	1.5	0.8	

the fact that the two prong nature is dominant only for the single-top background (see the discussion in Sec. IV E and, in particular, Fig. 11). In comparison, the signal tends to exhibit a more pronounced two prong nature (Fig. 9). For $m_B \gtrsim 2$ TeV, though, there is little advantage in applying S_4 , a consequence of the flattening of the τ_{21} distribution as discussed in Sec. IV E.

To further enhance the significance, we consider the invariant mass $M_{\text{inv}} \equiv m(J_Z, J_1)$, with J_1 defined as in selection S_2 . Since, for the signal events, these two jets are expected to have arisen from the decay of the B , we concentrate on intervals $|M_{\text{inv}} - m_B| \leq 3\Gamma_B$, for a given m_B . For $\kappa = 0.5$, the total widths Γ_B (as calculated in Sec. II C), for the benchmark points $m_B = 1.2, 1.8$ and 2.2 TeV are 32, 66.5 and 90 GeV respectively. As even a cursory examination of Table III shows, this restriction on M_{inv} is extremely useful in accentuating the signal-to-noise ratio. Calculated for an integrated luminosity of 300 fb^{-1} , the consequent discovery significances (defined as $\sigma \equiv S/\sqrt{B}$, where $S(B)$ represent the total number of signal (background) events) are also presented in Table III.

It is instructive to peruse Table III carefully. For one, the cut $S_4(a)$ would result in smaller significance values as compared to those for the alternative, namely, $S_4(b)$. This is just a vindication of our earlier argument that a stronger cut on the subjettness ratio τ_{21} preferentially removes the background events. An analogous (and expected) feature is afforded by a comparison with the significance reach for $R = 0.8$, presented in Table III for a cut of $\tau_{21} > 0.5$. With the Z -fatjet getting progressively more collimated as m_B increases, an increase in R (from 0.5 to 0.8) would not imply a significant increase in the number of signal events, catching only a few extra events with larger radiation. On the contrary, a much larger fraction of the background events, especially those accruing from top decays, would now be accepted by the algorithm, leading to a significant decrease in the ensuing significance.

2. The H -fatjet channel

We, now, consider the second possibility, namely when the vectorlike quark decays in the $B \rightarrow Hb$ channel. As we

have discussed earlier, $\text{Br}(B \rightarrow Hb) \approx \text{Br}(B \rightarrow Zb)$ and, with the hadronic branching fraction of the Higgs not being too different from that of the Z , nominally, the signal strengths should be similar. On the other hand, many of the SM backgrounds, such as those originating from W/Z or top-production, are expected to reduce drastically, on account of these peaking away from m_H . In other words, the naive expectation would be that this signal (comprising of one H -fatjet with two additional jets) would be significantly more visible against the background, as compared to that in the previous section. We would see, though, that this is borne out to a great extent, though not to the degree that a naive estimate would indicate.

With the mass difference $m_H - m_Z \ll m_B$, one would expect the signal profile to be quite similar in the two cases. Consequently, we retain all the earlier selection cuts, except for making the obvious alteration in S_2 , which, for the H -fatjet, now reads

$$m_J \in [110, 140] \text{ GeV} \quad \text{and} \quad p_T(J_H) > 500 \text{ GeV}. \quad (21)$$

The devolution of the cross section, as the selection criteria are applied consecutively, is summarized in Table IV for

TABLE IV. Top: the variation of the cross section for the H -fatjet signal ($B \rightarrow bH$) in (fb), for each of the BPs, as subsequent selection cuts are imposed for LHC operating at $\sqrt{s} = 13$ TeV. We use $\kappa = 0.5$ and $R = 0.5$. Bottom: the corresponding variation for the various contributions to the background.

m_B (TeV)	S_1	S_2	S_3	$S_4(a)$	$S_4(b)$
1.2	129.7	36.0	18.0	14.76	11.91
1.8	17.23	7.27	3.15	2.42	1.88
2.2	4.5	2.1	0.82	0.61	0.46
Backgrounds	S_1	S_2	S_3	$S_4(a)$	$S_4(b)$
$b\bar{b} + \text{jets}$	3.45×10^4	1.9×10^3	304	167	131
$V + \text{jets}$	7.5×10^3	339	65	43	31
$t\bar{t} + \text{jets}$	2.79×10^3	635	346	256	166
Others	356	42	3.2	2.4	2.0
Total	4.53×10^4	2.95×10^3	719	468	330

TABLE V. As in Table III but for H-fatjet ($B \rightarrow bH$) channel.

$R = 0.5, b\text{-jet} \geq 2$		After S_3			After $S_4(b)$		
$m_B \pm 3\Gamma_B$ (TeV)	$1.2 \pm 3\Gamma$	$1.8 \pm 3\Gamma$	$2.2 \pm 3\Gamma$	$1.2 \pm 3\Gamma$	$1.8 \pm 3\Gamma$	$2.2 \pm 3\Gamma$	
Signal(fb)	7.84	1.8	0.56	5.2	1.0	0.35	
Background(fb)	68.7	20.1	14.0	26.2	5.5	3.4	
Significance (σ_{300})	16.38	6.95	2.59	17.67	7.39	3.29	
$R = 0.8, b\text{-jet} \geq 2$		After S_3			After $S_4(b)$		
Significance (σ_{300})	12.2	5.1	1.2	12.5	5.0	1.2	

both the signal benchmark points as well as the backgrounds. Since our methodology is virtually identical to that in the preceding subsection, much of the details are very analogous, and we shall just concentrate on identifying the major differences.

That the backgrounds, on application of the cut S_1 alone, should remain identical to those in Table II is obvious. At this stage, the signal too remains very close to that in the previous case, a testament to the near equality of the raw signal strengths. This near equality is altered significantly on the imposition of S_2 , and is a consequence of the slightly higher mass of the Higgs as compared to the Z . Note that the demand for a two-prong jet of mass 110–140 GeV indirectly translates to a minimum p_T requirement (since $\Delta R \approx 2m_J/p_T$). Consequently a non-negligible fraction of events containing a putative fatjet with $p_T > 500$ GeV would no longer be reconstructed as one. Of course, this effect can be offset by allowing for a larger R . However, such a choice would also entail a larger background count. Furthermore, the somewhat flatter τ_{21} distribution that, say $R = 0.8$ entails (see Sec. IV E), renders the $S_4(a/b)$ cuts less effective.

S_3 , being only a requirement of the nonfatjet components of the event being b -tagged, understandably has nearly equal efficiency for the two channels. The small difference in efficiencies is attributable to the slightly different phase space distributions of the b emanating from the heavy B -decay. And while the S_4 cut is expected to have a different efficiency in the two cases, owing to a difference in the corresponding τ_{21} distributions, the effect is relatively small.

As in the preceding case, the significance can be further enhanced by restricting the invariant mass $M_{\text{inv}} \equiv m(J_H, J_1)$ to the interval $|M_{\text{inv}} - m_B| \leq 3\Gamma_B$. The consequent discovery significances, as calculated for an integrated luminosity of 300 fb^{-1} are presented in Table V. Note that we obtain marginally better significance in the J_H scenario for $m_B > 1.8$ TeV, compared to J_Z channel, primarily due to extra suppression of the background. Once again, a stronger cut on the subjettness ratio τ_{21} preferentially removes the background events and, for brevity's sake, we present the results only for $S_4(b)$. And, as in the previous case, the use of a larger R only serves to dilute the significance.

3. Discovery projection

It is interesting to note that, notwithstanding the differences in the effective efficiencies for the signal and background events, the two channels have very similar sensitivities. With the search strategy being very similar too, it is, thus, worthwhile to combine the two sets of results to reach an enhanced sensitivity and this is what we now embark on.

We demonstrate the significance as a function of m_B in Fig 13 for $\kappa = 0.5$ for an integrated luminosity of 300 fb^{-1} . It is $\geq 3\sigma$ for VLQ masses $< 2.2(2.0)$ TeV and $\geq 5\sigma$ for VLQ masses $< 2.05(1.84)$ TeV in the $J_H(J_Z)$ channel. Clearly, up to 1.6 TeV, both the channels predict almost same significance, but thereafter the H -fatjet channel is clearly the more sensitive one. This small difference in significance at smaller m_B values was expected because of the more restrictive nature of S_2 cut in the case of H , already discussed in Sec. IV F 2. Combining the two channels, the joint significance reach is $\geq 5\sigma$ ($\geq 3\sigma$) for VLQ masses $< 2.12(2.42)$ TeV. In Fig. 14 we have plotted the contours of 3σ and 5σ significance in the κ vs m_B plane for both J_Z and J_H channels. It is obvious from the plot that

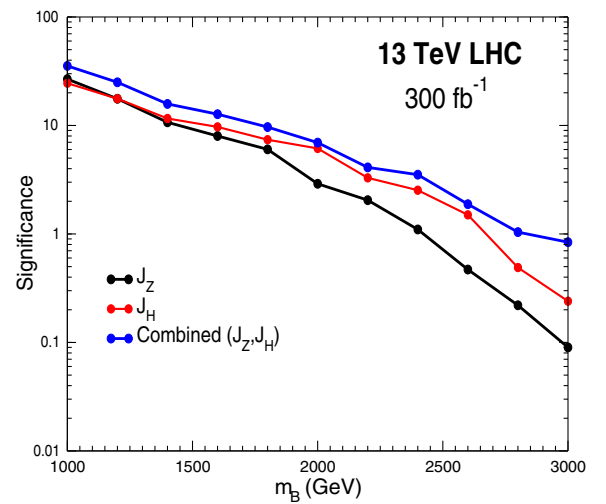


FIG. 13. Significance as a function of B mass, for two different fatjet scenario, Z and H , at 300 fb^{-1} luminosities for b -jets ≥ 2 and $S_4(b)$. We have assumed $R = 0.5$, $\kappa = 0.5$.

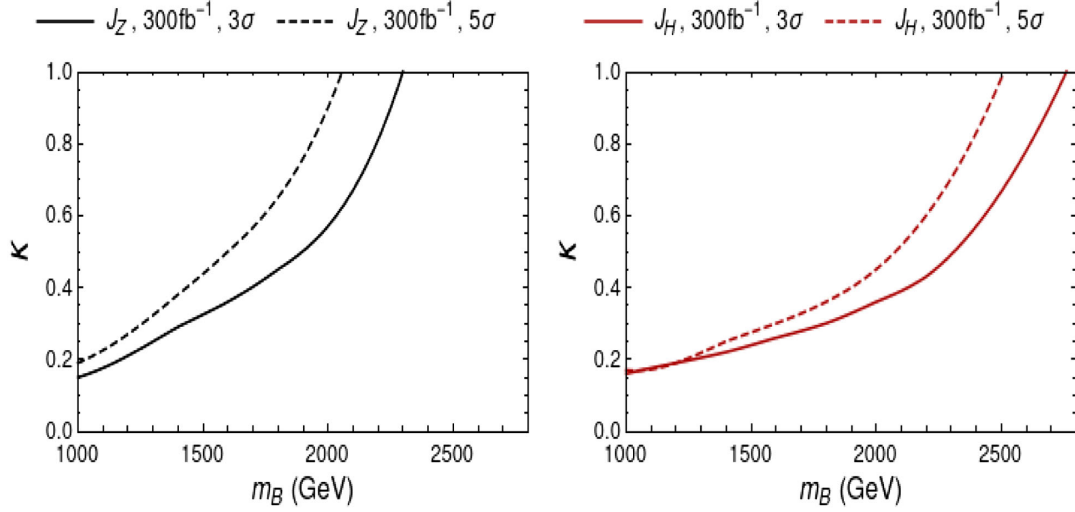


FIG. 14. Contours of 3σ and 5σ significances in the plane of κ vs m_B , at luminosity of 300 fb^{-1} for both J_Z (left) and J_H (right) fatjet case. Events are selected with b -jets ≥ 2 and $S_4(b)$. We have assumed $R = 0.5$.

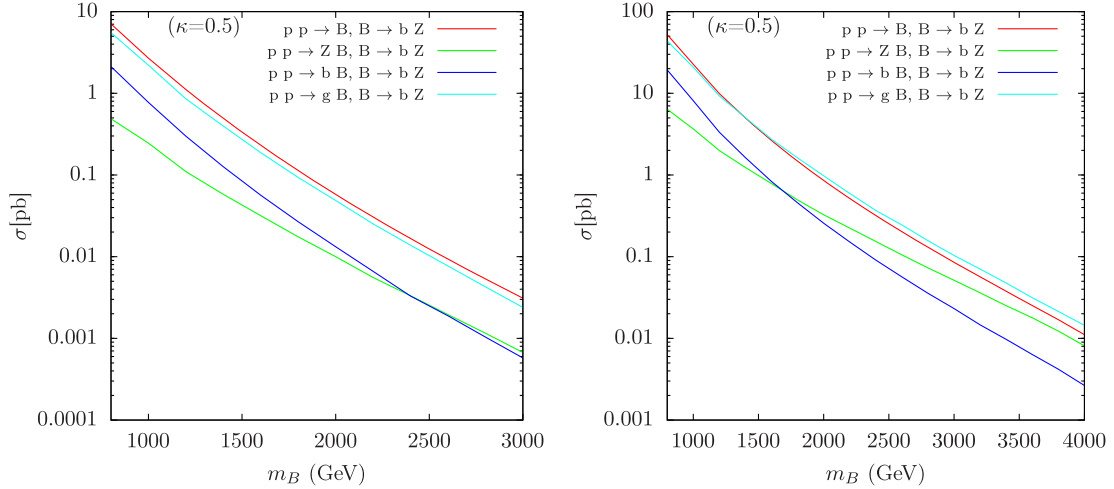


FIG. 15. Left: LO cross sections in 5FS using (NNPDF23LO1) for various relevant processes at 13 TeV. Right: same for a center of mass energy of 27 TeV.

with the J_H channel alone, it is possible to probe smaller values of κ with $3/5\sigma$ significance at a fixed m_B .

V. CONCLUSIONS AND OUTLOOK

Nonchiral (or vectorlike) fermions have been invoked in a multitude of theories, to address a medley of issues. The more theoretical concerns range from dynamical breaking of the electroweak symmetry or alleviating the little hierarchy problem in a class of theories to models providing a portal for dark matter. Concerns that are more immediate include explaining muon or electron anomalous magnetic moments or several puzzles in flavor physics. In particular, topless vectorlike doublets (B , Y) have been shown to provide a redressal of the tension between global

fits to electroweak precision tests and the forward backward asymmetry in $b\bar{b}$ production at LEP/SLC.

In our quest to examine the status of such resolutions, we begin by delineating the constraints on the mixings of the B with light counterparts, as obtained from measurements of electroweak precision variables and other flavor-sector processes. Such an exercise also helps determine the branching fractions for the B -quark decays. We, then, investigate possible LHC signatures of such a B -quark. The very structure of such theories imply a sizable a transition chromomagnetic moment κ , allowing for single-production such as $gg \rightarrow \bar{b}B$. Despite the smallness of κ , such a production channel could easily dominate QCD-driven pair production for significantly large m_B .

In this paper, we have concentrated on the single production of such a B in association with a bottom-jet, with the B , subsequently decaying to a Z/H boson and another b -jet. While such channels would be expected to be overwhelmed by large backgrounds (unless the Z decays hadronically), for a sufficiently large mass m_B (such as to evade the current experimental limits), the bosonic daughter is boosted so as to often manifest itself as a fatjet. Exploiting this feature, we have striven to identify both the kinematic features as well as the optimal jet reconstruction algorithms. In particular, the two-prong nature of the Z/H -fatjet is best evinced by the choice $R = 0.5$ for the radius parameter, rather than the more conventional $R = 0.8$. Complemented by the use of the subjetteness ratio τ_{21} as well as the imposition of a differential of cuts on the transverse momenta (a very stiff one for the fatjet and more moderate ones for the two subleading jets), the signal-to-background ratio can be improved to a great extent. As a final discriminator, we use the fact that the fatjet $J_{Z/H}$ and the jet with the maximal azimuthal separation from it should, preferentially, reconstruct the mass of the B .

The consequent significance ratio is quite handsome in either of the channels (Z/H) and, together, amount to more than 3σ for $m_B \sim 2.5$ TeV with an integrated luminosity of only 300 fb^{-1} . The HL-LHC option would, understandably, push the limit significantly. It is worthwhile to notice that it is the Higgs channel is the more sensitive one, a consequence of the twin facts that the branching fractions $\text{Br}(B \rightarrow b + Z/H)$ are very similar and that the SM backgrounds for the Higgs-fatjet channel are significantly smaller.

A key component of our search strategy is the requirement that at least two of the high- p_T jets, other than the fatjet, should be b -tagged (i.e., $N_b \geq 2$). While this was particularly useful in suppressing the SM backgrounds, the adoption of this criterion also meant that some of the potential signal processes too had to be left out as discussed in Sec. IV. Indeed, as Fig. 15 shows, the resonant production channel $pp \rightarrow B$ and even $pp \rightarrow gB$ have cross

sections significantly larger than that for the channel we worked with. However, with the QCD-multijet background now increasing manifolds, the pursuit of such channels would require analyses much more sophisticated than what we have used here. There is hope, though, that machine learning techniques could unmask the corresponding signal and we hope to return to this question at a later date.

Potentially much more interesting is the channel $pp \rightarrow BZ$. As can be seen from Fig. 15, while this rather subdominant for small m_B , for $m_B \gtrsim 2.3$ TeV it compares well with our channel and even overtakes it. While one b -jet is now lost, it is now compensated by a Z (H), which has its own distinct signature, even for hadronic decays. This, potentially would substantially increase the signal-to-background ratio, primarily on account of a much reduced background.

Similarly, the production of a much heavier B (than what we have considered) is severely suppressed at the LHC. This, though, would not be the case at a future circular collider. In particular, note that the $pp \rightarrow BZ$ mode now dominates over our chosen mode starting with a much smaller m_B . However, such a machine would have its own imprint on multiple issues such as the nature of QCD radiation, the efficiencies etc., and a naive extension of our analysis would not be tenable. In particular, new jet substructure observables might be called for. These are only a subset of open questions that we hope to address in future.

ACKNOWLEDGMENTS

The authors thank Brajesh Choudhary for access to computers brought under the aegis of the Grant No. SR-MF/PS-02I2014-DUB (G) of the DST (India). K. D. acknowledges Council for Scientific and Industrial Research (CSIR), India for JRF/SRF fellowship with the award letter no. 09/045(1654)/2019-EMR-I. N. K. acknowledges the support from the Dr. D.S. Kothari Postdoctoral scheme (201819-PH/18-19/0013).

-
- [1] ALEPH, CDF, D0, DELPHI, L3, OPAL, SLD, LEP Electroweak Working Group, Tevatron Electroweak Working Group, SLD Electroweak, and Heavy Flavour Groups Collaborations, Precision electroweak measurements and constraints on the Standard Model, [arXiv: 1012.2367](https://arxiv.org/abs/1012.2367).
 - [2] P.D. Group, Review of particle physics*, [Prog. Theor. Exp. Phys. \(2020\)](https://arxiv.org/abs/2008.08865), 083C01.
 - [3] G. Aad *et al.* (ATLAS Collaboration), Observation of a new particle in the search for the Standard Model Higgs

boson with the ATLAS detector at the LHC, [Phys. Lett. B **716**, 1 \(2012\)](https://arxiv.org/abs/1207.3217).

- [4] S. Chatrchyan *et al.* (CMS Collaboration), Observation of a new boson at a mass of 125 GeV with the CMS Experiment at the LHC, [Phys. Lett. B **716**, 30 \(2012\)](https://arxiv.org/abs/1207.3217).
- [5] B. Abi, T. Albahri, S. Al-Kilani, D. Allspach, L. P. Alonzi, A. Anastasi *et al.* (Muon $g-2$ Collaboration), Measurement of the Positive Muon Anomalous Magnetic Moment to 0.46 ppm, [Phys. Rev. Lett. **126**, 141801 \(2021\)](https://arxiv.org/abs/2106.13273).

- [6] Y. Amhis *et al.* (HFLAV Collaboration), Averages of b -hadron, c -hadron, and τ -lepton properties as of summer 2016, *Eur. Phys. J. C* **77**, 895 (2017).
- [7] J. Aguilar-Saavedra, R. Benbrik, S. Heinemeyer, and M. Pérez-Victoria, Handbook of vectorlike quarks: Mixing and single production, *Phys. Rev. D* **88**, 094010 (2013).
- [8] S. A. Ellis, R. M. Godbole, S. Gopalakrishna, and J. D. Wells, Survey of vector-like fermion extensions of the Standard Model and their phenomenological implications, *J. High Energy Phys.* **09** (2014) 130.
- [9] J. Kang, P. Langacker, and B. D. Nelson, Theory and phenomenology of exotic isosinglet quarks and squarks, *Phys. Rev. D* **77**, 035003 (2008).
- [10] R. Dermisek, Unification of gauge couplings in the standard model with extra vectorlike families, *Phys. Rev. D* **87**, 055008 (2013).
- [11] B. Bhattacharjee, P. Byakti, A. Kushwaha, and S. K. Vempati, Unification with vector-like fermions and signals at LHC, *J. High Energy Phys.* **05** (2018) 090.
- [12] D. Emmanuel-Costa and R. Gonzalez Felipe, Minimal string-scale unification of gauge couplings, *Phys. Lett. B* **623**, 111 (2005).
- [13] V. Barger, J. Jiang, P. Langacker, and T. Li, String scale gauge coupling unification with vector-like exotics and non-canonical $U(1)(Y)$ normalization, *Int. J. Mod. Phys. A* **22**, 6203 (2007).
- [14] I. Dorsner, S. Fajfer, and I. Mustac, Light vector-like fermions in a minimal $SU(5)$ setup, *Phys. Rev. D* **89**, 115004 (2014).
- [15] S. Choi, D. Choudhury, A. Freitas, J. Kalinowski, J. Kim, and P. Zerwas, Dirac neutralinos and electroweak scalar bosons of $N = 1/N = 2$ hybrid supersymmetry at colliders, *J. High Energy Phys.* **08** (2010) 025.
- [16] S. Choi, D. Choudhury, A. Freitas, J. Kalinowski, and P. Zerwas, The extended Higgs system in R -symmetric supersymmetry theories, *Phys. Lett. B* **697**, 215 (2011); Erratum, **698**, 457 (2011).
- [17] S. P. Martin, Extra vector-like matter and the lightest Higgs scalar boson mass in low-energy supersymmetry, *Phys. Rev. D* **81**, 035004 (2010).
- [18] S. P. Martin, Raising the Higgs mass with Yukawa couplings for isotriplets in vector-like extensions of minimal supersymmetry, *Phys. Rev. D* **82**, 055019 (2010).
- [19] P. W. Graham, A. Ismail, S. Rajendran, and P. Saraswat, A little solution to the little hierarchy problem: A vector-like generation, *Phys. Rev. D* **81**, 055016 (2010).
- [20] T. Moroi, R. Sato, and T. T. Yanagida, Extra matters decree the relatively heavy Higgs of mass about 125 GeV in the supersymmetric model, *Phys. Lett. B* **709**, 218 (2012).
- [21] M. Endo, K. Hamaguchi, S. Iwamoto, and N. Yokozaki, Higgs mass, muon $g-2$, and LHC prospects in gauge mediation models with vector-like matters, *Phys. Rev. D* **85**, 095012 (2012).
- [22] S. P. Martin and J. D. Wells, Implications of gauge-mediated supersymmetry breaking with vector-like quarks and a ~ 125 GeV Higgs boson, *Phys. Rev. D* **86**, 035017 (2012).
- [23] W. Fischler and W. Tangarife, Vector-like fields, messenger mixing and the Higgs mass in gauge mediation, *J. High Energy Phys.* **05** (2014) 151.
- [24] B. A. Dobrescu and C. T. Hill, Electroweak Symmetry Breaking Via Top Condensation Seesaw, *Phys. Rev. Lett.* **81**, 2634 (1998).
- [25] R. Chivukula, B. A. Dobrescu, H. Georgi, and C. T. Hill, Top quark seesaw theory of electroweak symmetry breaking, *Phys. Rev. D* **59**, 075003 (1999).
- [26] H.-J. He, T. M. Tait, and C. Yuan, New top flavor models with seesaw mechanism, *Phys. Rev. D* **62**, 011702.
- [27] R. Contino, L. Da Rold, and A. Pomarol, Light custodians in natural composite Higgs models, *Phys. Rev. D* **75**, 055014 (2007).
- [28] C. Anastasiou, E. Furlan, and J. Santiago, Realistic composite Higgs models, *Phys. Rev. D* **79**, 075003 (2009).
- [29] N. Vignaroli, Discovering the composite Higgs through the decay of a heavy fermion, *J. High Energy Phys.* **07** (2012) 158.
- [30] A. De Simone, O. Matsedonskyi, R. Rattazzi, and A. Wulzer, A first top partner Hunter's guide, *J. High Energy Phys.* **04** (2013) 004.
- [31] C. Delaunay, C. Grojean, and G. Perez, Modified Higgs physics from composite light flavors, *J. High Energy Phys.* **09** (2013) 090.
- [32] Marc Gillioz, Ramona Gröber, Andreas Kapuvari, and Margarete Mühlleitner, Vector-like bottom quarks in composite Higgs models, *J. High Energy Phys.* **03** (2014) 037.
- [33] A. Banerjee, G. Bhattacharyya, N. Kumar, and T. S. Ray, Constraining composite Higgs models using LHC data, *J. High Energy Phys.* **03** (2018) 062.
- [34] T. Han, H. E. Logan, B. McElrath, and L.-T. Wang, Phenomenology of the little Higgs model, *Phys. Rev. D* **67**, 095004 (2003).
- [35] M. Carena, J. Hubisz, M. Perelstein, and P. Verdier, Collider signature of T-quarks, *Phys. Rev. D* **75**, 091701 (2007).
- [36] D. Choudhury and D. K. Ghosh, LHC signals of T-odd heavy quarks in the littlest Higgs model, *J. High Energy Phys.* **08** (2007) 084.
- [37] S. Choudhury, A. S. Cornell, A. Deandrea, N. Gaur, and A. Goyal, Lepton flavour violation in the little Higgs model, *Phys. Rev. D* **75**, 055011 (2007).
- [38] S. Matsumoto, T. Moroi, and K. Tobe, Testing the littlest Higgs model with T-parity at the large hadron collider, *Phys. Rev. D* **78**, 055018 (2008).
- [39] D. Choudhury, D. K. Ghosh, and S. K. Rai, Dijet signals of the little Higgs model with T-parity, *J. High Energy Phys.* **07** (2012) 013.
- [40] J. Berger, J. Hubisz, and M. Perelstein, A fermionic top partner: Naturalness and the LHC, *J. High Energy Phys.* **07** (2012) 016.
- [41] B. Patt and F. Wilczek, Higgs-field portal into hidden sectors, [arXiv:hep-ph/0605188](https://arxiv.org/abs/hep-ph/0605188).
- [42] S. Gopalakrishna, S. J. Lee, and J. D. Wells, Dark matter and Higgs boson collider implications of fermions in an abelian-gauged hidden sector, *Phys. Lett. B* **680**, 88 (2009).
- [43] S. Baek, P. Ko, and W.-I. Park, Search for the Higgs portal to a singlet fermionic dark matter at the LHC, *J. High Energy Phys.* **02** (2012) 047.

- [44] E. J. Chun and T. Mondal, Explaining $g - 2$ anomalies in two Higgs doublet model with vector-like leptons, *J. High Energy Phys.* **11** (2020) 077.
- [45] K. Kowalska and E. M. Sessolo, Expectations for the muon $g-2$ in simplified models with dark matter, *J. High Energy Phys.* **09** (2017) 112.
- [46] K. Ishiwata, Z. Ligeti, and M. B. Wise, New vector-like fermions and flavor physics, *J. High Energy Phys.* **10** (2015) 027.
- [47] B. Barman, D. Borah, L. Mukherjee, and S. Nandi, Correlating the anomalous results in $b \rightarrow s$ decays with inert Higgs doublet dark matter and muon ($g - 2$), *Phys. Rev. D* **100**, 115010 (2019).
- [48] A. Crivellin, C. A. Manzari, M. Alguero, and J. Matias, Combined Explanation of the $Z \rightarrow b\bar{b}$ Forward-Backward Asymmetry, the Cabibbo Angle Anomaly, $\tau \rightarrow \mu\nu\nu$ and $b \rightarrow s\ell^+\ell^-$ Data, *Phys. Rev. Lett.* **127**, 011801 (2021).
- [49] K. Cheung, W.-Y. Keung, C.-T. Lu, and P.-Y. Tseng, Vector-like quark interpretation for the CKM unitarity violation, excess in Higgs signal strength, and bottom quark forward-backward asymmetry, *J. High Energy Phys.* **05** (2020) 117.
- [50] D. Choudhury, T. M. Tait, and C. Wagner, Beautiful mirrors and precision electroweak data, *Phys. Rev. D* **65**, 053002 (2002).
- [51] M. S. Chanowitz, $Z \rightarrow b\bar{b}$ Decay Asymmetry: Lose-Lose for the Standard Model, *Phys. Rev. Lett.* **87**, 231802 (2001).
- [52] M. Buchkremer, G. Cacciapaglia, A. Deandrea, and L. Panizzi, Model independent framework for searches of top partners, *Nucl. Phys.* **B876**, 376 (2013).
- [53] J. Nutter, R. Schwienhorst, D. G. Walker, and J.-H. Yu, Single top production as a probe of B-prime quarks, *Phys. Rev. D* **86**, 094006 (2012).
- [54] X. Gong, C.-X. Yue, and Y.-C. Guo, Search for vector-like bottom quark via Zb production at the LHC, *Phys. Lett. B* **793**, 175 (2019).
- [55] H. Cai, Mono vector-quark production at the LHC, *J. High Energy Phys.* **02** (2013) 104.
- [56] ATLAS Collaboration, Search for single production of a vector-like B quark decaying into a bottom quark and a Higgs boson which decays into a pair of photons.
- [57] M. Aaboud *et al.* (ATLAS Collaboration), Combination of the Searches for Pair-Produced Vector-Like Partners of the Third-Generation Quarks at $\sqrt{s} = 13$ TeV with the ATLAS Detector, *Phys. Rev. Lett.* **121**, 211801 (2018).
- [58] A. M. Sirunyan *et al.* (CMS Collaboration), Search for single production of vector-like quarks decaying to a top quark and a W boson in proton-proton collisions at $\sqrt{s} = 13$ TeV, *Eur. Phys. J. C* **79**, 90 (2019).
- [59] A. M. Sirunyan *et al.* (CMS Collaboration), Search for excited quarks of light and heavy flavor in $\gamma + \text{jet}$ final states in proton-proton collisions at $\sqrt{s} = 13$ TeV, *Phys. Lett. B* **781**, 390 (2018).
- [60] S. Bhattacharya, S. S. Chauhan, B. C. Choudhary, and D. Choudhury, Search for excited quarks in $q\bar{q} \rightarrow \gamma\gamma$ at the LHC, *Phys. Rev. D* **76**, 115017 (2007).
- [61] S. Bhattacharya, S. S. Chauhan, B. C. Choudhary, and D. Choudhury, Quark excitations through the prism of direct photon plus jet at the LHC, *Phys. Rev. D* **80**, 015014 (2009).
- [62] V. Khachatryan *et al.* (CMS Collaboration), Search for excited quarks in the $\gamma + \text{jet}$ final state in proton-proton collisions at $\sqrt{s} = 8$ TeV, *Phys. Lett. B* **738**, 274 (2014).
- [63] A. M. Sirunyan *et al.* (CMS Collaboration), Search for vector-like quarks in events with two oppositely charged leptons and jets in proton-proton collisions at $\sqrt{s} = 13$ TeV, *Eur. Phys. J. C* **79**, 364 (2019).
- [64] A. M. Sirunyan *et al.* (CMS Collaboration), Search for single production of vector-like quarks decaying to a b quark and a Higgs boson, *J. High Energy Phys.* **06** (2018) 031.
- [65] A. M. Sirunyan *et al.* (CMS Collaboration), Search for vector-like T and B quark pairs in final states with leptons at $\sqrt{s} = 13$ TeV, *J. High Energy Phys.* **08** (2018) 177.
- [66] A. Buckley, J. Butterworth, L. Corpe, D. Huang, and P. Sun, New sensitivity of current LHC measurements to vector-like quarks, *SciPost Phys.* **9**, 069 (2020).
- [67] S. Chatrchyan *et al.* (CMS Collaboration), Inclusive search for a vector-like t quark with charge $\frac{2}{3}$ in pp collisions at $\sqrt{s} = 8$ TeV, *Phys. Lett. B* **729**, 149 (2014).
- [68] V. Khachatryan *et al.* (CMS Collaboration), Search for vector-like T quarks decaying to top quarks and Higgs bosons in the all-hadronic channel using jet substructure, *J. High Energy Phys.* **06** (2015) 080.
- [69] G. Aad *et al.* (ATLAS Collaboration), Search for the production of single vector-like and excited quarks in the Wt final state in pp collisions at $\sqrt{s} = 8$ TeV with the ATLAS detector, *J. High Energy Phys.* **02** (2016) 110.
- [70] G. Aad *et al.* (ATLAS Collaboration), Search for single production of vector-like quarks decaying into Wb in pp collisions at $\sqrt{s} = 8$ TeV with the ATLAS detector, *Eur. Phys. J. C* **76**, 442 (2016).
- [71] S. Schael *et al.* (ALEPH, DELPHI, L3, OPAL, SLD, LEP Electroweak Working Group, SLD Electroweak Group, SLD Heavy Flavour Group Collaboration), Precision electroweak measurements on the Z resonance, *Phys. Rep.* **427**, 257 (2006).
- [72] G. Aad *et al.* (ATLAS Collaboration), Combined measurements of Higgs boson production and decay using up to 80 fb^{-1} of proton-proton collision data at $\sqrt{s} = 13$ TeV collected with the ATLAS experiment, *Phys. Rev. D* **101**, 012002 (2020).
- [73] J. W. Nutter, R. Schwienhorst, D. G. E. Walker, and J.-H. Yu, Single top production as a probe of B' quarks, *Phys. Rev. D* **86**, 094006 (2012).
- [74] W. Skiba and D. Tucker-Smith, Using jet mass to discover vector quarks at the LHC, *Phys. Rev. D* **75**, 115010 (2007).
- [75] V. Khachatryan *et al.* (CMS Collaboration), Identification techniques for highly boosted W bosons that decay into hadrons, *J. High Energy Phys.* **12** (2014) 017.
- [76] J. M. Butterworth, J. R. Ellis, A. R. Raklev, and G. P. Salam, Discovering Baryon-Number Violating Neutralino Decays at the LHC, *Phys. Rev. Lett.* **103**, 241803 (2009).
- [77] ATLAS Collaboration, A method for discovering heavy particles decaying into single boosted jets with substructure using the k_{\perp} algorithm.
- [78] S. Schätzel, Boosted top quarks and jet structure, *Eur. Phys. J. C* **75**, 415 (2015).

- [79] J. M. Butterworth, A. R. Davison, M. Rubin, and G. P. Salam, Jet Substructure as a New Higgs Search Channel at the LHC, *Phys. Rev. Lett.* **100**, 242001 (2008).
- [80] ATLAS Collaboration, ATLAS sensitivity to the Standard Model Higgs in the HW and HZ channels at high transverse momenta.
- [81] A. M. Sirunyan *et al.* (CMS Collaboration), Search for massive resonances decaying into WW, WZ or ZZ bosons in proton-proton collisions at $\sqrt{s} = 13$ TeV, *J. High Energy Phys.* **03** (2017) 162.
- [82] CMS Collaboration, A Cambridge-Aachen (C-A) based jet algorithm for boosted top-jet tagging.
- [83] M. Cacciari, G. P. Salam, and G. Soyez, The anti- k_t jet clustering algorithm, *J. High Energy Phys.* **04** (2008) 063.
- [84] S. D. Ellis, C. K. Vermilion, and J. R. Walsh, Techniques for improved heavy particle searches with jet substructure, *Phys. Rev. D* **80**, 051501 (2009).
- [85] S. D. Ellis, C. K. Vermilion, and J. R. Walsh, Recombination algorithms and jet substructure: Pruning as a tool for heavy particle searches, *Phys. Rev. D* **81**, 094023 (2010).
- [86] A. J. Larkoski, S. Marzani, G. Soyez, and J. Thaler, Soft drop, *J. High Energy Phys.* **05** (2014) 146.
- [87] A. M. Sirunyan *et al.* (CMS Collaboration), Search for massive resonances decaying into WW, WZ, ZZ, qW , and qZ with dijet final states at $\sqrt{s} = 13$ TeV, *Phys. Rev. D* **97**, 072006 (2018).
- [88] CMS Collaboration, Jet algorithms performance in 13 TeV data.
- [89] R. Kogler *et al.*, Jet substructure at the large hadron collider: Experimental review, *Rev. Mod. Phys.* **91**, 045003 (2019).
- [90] A. Sirunyan *et al.* (CMS Collaboration), Search for pair production of vector-like T and B quarks in single-lepton final states using boosted jet substructure in proton-proton collisions at $\sqrt{s} = 13$ TeV, *J. High Energy Phys.* **11** (2017) 085.
- [91] A. M. Sirunyan *et al.* (CMS Collaboration), Search for electroweak production of a vector-like quark decaying to a top quark and a Higgs boson using boosted topologies in fully hadronic final states, *J. High Energy Phys.* **04** (2017) 136.
- [92] J. Thaler and K. Van Tilburg, Identifying boosted objects with N-subjettiness, *J. High Energy Phys.* **03** (2011) 015.
- [93] R. D. Ball *et al.*, Parton distributions with LHC data, *Nucl. Phys.* **B867**, 244 (2013).
- [94] G. Cacciapaglia, A. Carvalho, A. Deandrea, T. Flacke, B. Fuks, D. Majumder *et al.*, Next-to-leading-order predictions for single vector-like quark production at the LHC, *Phys. Lett. B* **793**, 206 (2019).
- [95] S. Catani, L. Cieri, G. Ferrera, D. de Florian, and M. Grazzini, Vector Boson Production at Hadron Colliders: A Fully Exclusive QCD Calculation at NNLO, *Phys. Rev. Lett.* **103**, 082001 (2009).
- [96] S. Catani and M. Grazzini, An NNLO Subtraction Formalism in Hadron Collisions and Its Application to Higgs Boson Production at the LHC, *Phys. Rev. Lett.* **98**, 222002 (2007).
- [97] G. Balossini, G. Montagna, C. M. Carloni Calame, M. Moretti, O. Nicrosini, F. Piccinini *et al.*, Combination of electroweak and QCD corrections to single W production at the Fermilab Tevatron and the CERN LHC, *J. High Energy Phys.* **01** (2010) 013.
- [98] C. Muselli, M. Bonvini, S. Forte, S. Marzani, and G. Ridolfi, Top quark pair production beyond NNLO, *J. High Energy Phys.* **08** (2015) 076.
- [99] S. Chatrchyan *et al.* (CMS Collaboration), Identification of b-quark jets with the CMS Experiment, *J. Instrum.* **8**, P04013 (2013).
- [100] G. Aad *et al.* (ATLAS Collaboration), Measurement of the inclusive and dijet cross-sections of b^- jets in pp collisions at $\sqrt{s} = 7$ TeV with the ATLAS detector, *Eur. Phys. J. C* **71**, 1846 (2011).
- [101] J. Alwall, R. Frederix, S. Frixione, V. Hirschi, F. Maltoni, O. Mattelaer *et al.*, The automated computation of tree-level and next-to-leading order differential cross sections, and their matching to parton shower simulations, *J. High Energy Phys.* **07** (2014) 079.
- [102] J. M. Campbell, R. Ellis, and C. Williams, Vector boson pair production at the LHC, *J. High Energy Phys.* **07** (2011) 018.
- [103] G. Aad *et al.* (ATLAS Collaboration), Measurement of the associated production of a Higgs boson decaying into b -quarks with a vector boson at high transverse momentum in pp collisions at $\sqrt{s} = 13$ TeV with the ATLAS detector, *Phys. Lett. B* **816**, 136204 (2021).
- [104] N. Kidonakis, Theoretical results for electroweak-boson and single-top production, *Proc. Sci.*, DIS2015 (2015) 170 [arXiv:1506.04072].
- [105] A. Alloul, N. D. Christensen, C. Degrande, C. Duhr, and B. Fuks, FeynRules 2.0—A complete toolbox for tree-level phenomenology, *Comput. Phys. Commun.* **185**, 2250 (2014).
- [106] N. D. Christensen and C. Duhr, FeynRules—Feynman rules made easy, *Comput. Phys. Commun.* **180**, 1614 (2009).
- [107] J. Alwall, M. Herquet, F. Maltoni, O. Mattelaer, and T. Stelzer, MADGRAPH5: Going beyond, *J. High Energy Phys.* **06** (2011) 128.
- [108] T. Sjostrand, S. Mrenna, and P. Z. Skands, PYTHIA6.4 physics and manual, *J. High Energy Phys.* **05** (2006) 026.
- [109] M. L. Mangano, M. Moretti, F. Piccinini, and M. Treccani, Matching matrix elements and shower evolution for top-quark production in hadronic collisions, *J. High Energy Phys.* **01** (2007) 013.
- [110] S. Hoeche, F. Krauss, N. Lavesson, L. Lonnblad, M. Mangano, A. Schaliche *et al.*, Matching parton showers and matrix elements, in *HERA and the LHC: A Workshop on the Implications of HERA for LHC Physics: CERN—DESY Workshop 2004/2005* (Midterm Meeting, CERN, 2004; Final Meeting, DESY, 2005) (2005), pp. 288–289.
- [111] J. Alwall *et al.*, Comparative study of various algorithms for the merging of parton showers and matrix elements in hadronic collisions, *Eur. Phys. J. C* **53**, 473 (2008).
- [112] J. Alwall, S. de Visscher, and F. Maltoni, QCD radiation in the production of heavy colored particles at the LHC, *J. High Energy Phys.* **02** (2009) 017.
- [113] J. de Favereau, C. Delaere, P. Demin, A. Giammanco, V. Lemaître, A. Mertens *et al.* (DELPHES 3 Collaboration), DELPHES 3, A modular framework for fast simulation of

- a generic collider experiment, *J. High Energy Phys.* **02** (2014) 057.
- [114] M. Cacciari, G.P. Salam, and G. Soyez, FastJet user manual, *Eur. Phys. J. C* **72**, 1896 (2012).
- [115] M. Aaboud *et al.* (ATLAS Collaboration), Operation and performance of the ATLAS Tile Calorimeter in Run 1, *Eur. Phys. J. C* **78**, 987 (2018).
- [116] S. Goy López (CMS Collaboration), CMS detector performance, *EPJ Web Conf.* **182**, 02076 (2018).
- [117] J. Shelton, Jet substructure, in *Theoretical Advanced Study Institute in Elementary Particle Physics: Searching for New Physics at Small and Large Scales* (2013), pp. 303–340 [[arXiv:1302.0260](#)].